Targeting the extra domain A of fibronectin for cancer therapy with CAR-T cells

Celia Martín-Otal,[1] Aritz Lasarte-Cia,[1] Diego Serrano,[2] Noelia Casares,[1] Enrique Conde,[1] Flor Navarro,[1] Inés Sánchez-Moreno,[1] Marta Gorraiz,[1] Patricia Sarrión,[1] Alfonso Calvo [ID],[2] Carlos E De Andrea,[3,4] José Echeveste,[4] Amaia Vilas,[5] Juan Roberto Rodriguez-Madoz,[3,5,6] Jesús San Miguel,[3,5,6,7,8] Felipe Prosper,[3,5,6,7,8] Sandra Hervas-Stubbs [ID],[1,3] Juan Jose Lasarte [ID],[1,3,8] Teresa Lozano[1,3]

For numbered affiliations see end of article.

Correspondence to
Dr Juan Jose Lasarte;
jjlasarte@unav.es

Dr Teresa Lozano;
tlmoreda@unav.es

ABSTRACT

Background One of the main difficulties of adoptive cell therapies with chimeric antigen receptor (CAR)-T cells in solid tumors is the identification of specific target antigens. The tumor microenvironment can present suitable antigens for CAR design, even though they are not expressed by the tumor cells. We have generated a CAR specific for the splice variant extra domain A (EDA) of fibronectin, which is highly expressed in the tumor stroma of many types of tumors but not in healthy tissues.

Methods EDA expression was explored in RNA-seq data from different human tumor types and by immunohistochemistry in paraffin-embedded tumor biopsies. Murine and human anti-EDA CAR-T cells were prepared using recombinant retro/lentiviruses, respectively. The functionality of EDA CAR-T cells was measured in vitro in response to antigen stimulation. The antitumor activity of EDA CAR-T cells was measured in vivo in C57BL/6 mice challenged with PM299L-EDA hepatocarcinoma cell line, in 129Sv mice-bearing F9 teratocarcinoma and in NSG mice injected with the human hepatocarcinoma cell line PLC.

Results EDA CAR-T cells recognized and killed EDA-expressing tumor cell lines in vitro and rejected EDA-expressing tumors in immunocompetent mice. Notably, EDA CAR-T cells showed an antitumor effect in mice injected with EDA-negative tumor cells lines when the tumor stroma or the basement membrane of tumor endothelial cells express EDA. Thus, EDA CAR-T administration delayed tumor growth in immunocompetent 129Sv mice challenged with teratocarcinoma cell line F9. EDA CAR-T treatment exerted an antiangiogenic effect and significantly reduced gene signatures associated with epithelial-mesenchymal transition, collagen synthesis, extracellular matrix organization as well as IL-6-STAT5 and KRAS pathways. Importantly, the human version of EDA CAR, that includes the human 41BB and CD3ζ endodomains, exerted strong antitumor activity in NSG mice challenged with the human hepatocarcinoma cell line PLC, which expresses EDA in the tumor stroma and the endothelial vasculature. EDA CAR-T cells exhibited a tropism for EDA-expressing tumor tissue and no toxicity was observed in tumor bearing or in healthy mice.

Conclusions These results suggest that targeting the tumor-specific fibronectin splice variant EDA with CAR-T

WHAT IS ALREADY KNOWN ON THIS TOPIC

⇒ The aberrant tumor vasculature and the complexity of the extracellular matrix, with excessive intratumoral deposition of collagen or fibronectins, in addition to the difficulty in identifying specific tumor antigens to be targeted with chimeric antigen receptor T-cell (CAR-T) makes challenging the design of effective CAR-T for solid tumors.

⇒ In this effort, it is necessary to explore other alternative antigens present in the tumor microenvironment, even if they are not expressed by the tumor cell itself.

WHAT THIS STUDY ADDS

⇒ We identified the extra domain A (EDA) from fibronectin as a potential target antigen for CAR-T cell design.

⇒ EDA CAR-T cell-based therapy induced significant changes in the tumor microenvironment and exerted antitumor activity in murine tumors models expressing EDA in the tumor extracellular matrix or the basement membrane of the tumor endothelium.

HOW THIS STUDY MIGHT AFFECT RESEARCH, PRACTICE AND/OR POLICY

⇒ Human EDA CAR-T cells exerted a strong antitumoral effect in an NSG xenograft model for human hepatocarcinoma, suggesting a potential translation to human settings for the treatment of human tumors with upregulated EDA expression.

cells is feasible and offers a therapeutic option that is applicable to different types of cancer.

INTRODUCTION

Chimeric antigen receptor T-cell (CAR-T) therapy has shown encouraging antitumor efficacy in some hematological tumors[1 2] and constitutes a very promising advanced therapy for the treatment of cancer. However, the initial response rates achieved with the current

generation of anti-CD19 CAR-T cells in certain malignant B-cell tumors do not apply equally to other hematological cancers and much less to solid tumors, where many challenges still need to be overcome.[3] The complexity of the extracellular matrix (ECM) of tumors, with excessive intratumoral deposition of collagen, fibronectins, laminins or hyaluronan leads to inefficient homing and tumor penetration of redirected T cells.[4–7] For these reasons, tumor ECM components not commonly found in healthy tissues are considered as therapeutic targets for cancer.

During cancer progression, the ECM undergoes dramatic changes which promote cancer cell migration and invasion. In the remodeled tumor ECM, fibronectin (FN) acts as a central organizer of ECM molecules and mediates the crosstalk between the tumor microenvironment and cancer cells.[8] Although FN is encoded by a single gene, the alternative splicing of its pre-mRNA and the incorporation of extra domains result in the formation of cell- and tissue-specific FN isoforms. Splicing occurs at three sites, with the possibility of incorporating the extra domain A (EDA), extra domain B (EDB), or the IIICS domain. Fibronectin isoforms comprizing the EDA or EDB domains are also known as oncofetal forms because they are expressed during embryonic development, restricted in normal adult tissues and re-expressed in adults during cancer progression.[9] These spliced versions of FN present in the ECM belong to cellular fibronectin type and are not present in soluble plasma fibronectin. We focused on EDA as a potential target antigen for CAR-T cell development since it has been reported to be highly expressed many tumor types as compared with normal tissues[10] and this increased expression is correlated with cancer progression, dissemination and poor prognosis. Interestingly, antibody-cytokine or antibody-enzyme conjugates based on EDA-specific monoclonal antibodies have shown potent antitumor activity in preclinical animal models.[11 12] Collectively, these data highlight EDA as an attractive target for CAR design.

We generated EDA-specific CAR-T cells that were tested in vitro and in vivo for their capacity to reject tumors.

We demonstrate that EDA CAR-T cells recognize EDA in an antigen-dependent manner and display antitumor activity in vivo in several murine tumor models, such as immunocompetent mice-bearing F9 teratocarcinoma or NSG mice challenged with the human hepatocarcinoma cell line PLC.

MATERIALS AND METHODS
Data acquisition
Data from TCGA samples for 15 different tumor types and adjacent normal samples were explored for changes of alternative splicing events (exon 33 skip (EDA)) using SpliceSeq tool (V.2.1)[13] (http://projects.insilico.us.com/TCGASpliceSeq/). Only pair samples including also the EDA expression in the normal tissue surrounding the tumor were considered. The percent-splice-in (PSI)

value was calculated to quantify alternative splicing events ranging from 0 to 1 in TCGA SpliceSeq[14] (PSI is the ratio of normalized read counts indicating inclusion of EDA element over the total normalized reads for that event (both inclusion and exclusion reads)). EDA alternative splicing events were also evaluated in a cohort of 17 hepatocellular carcinoma (HCC) patients with available RNASeq data from our institution. The ratio between the expression levels (read counts) of exon 33 (EDA) and exon 34 (included in all fibronectin isoforms) in both tumor and normal hepatic tissue was used as an estimation of EDA expression in HCC.

Mice
Female C57BL/6J mice were purchased from Harlan Laboratories. 129Sv mice were obtained from Janvier Laboratory (Le Genest Saint Isle, France). NOD scid gamma (NSG) mice were bred in our animal facilities at the Centro de Investigación Médica Aplicada.

Cell lines
The murine HCC PM299L (provided by Dr. Lujambio, NY), the murine melanoma B16F10 (American Type Culture Collection, ATCC), the human hepatocarcinoma PLC and HUH7 and the human cholangiocarcinoma HUCCT and TFK1 cell lines (provided by Dr. Ávila, Pamplona, Spain) were cultured in complete medium (RPMI 1640 or DMEM containing 10% FCS, antibiotics, 2 mM glutamine and 50 µM 2-ME). Jurkat cells transfected with a triple parameter reporter (TPR) system, provided by Dr Hudecek (Würzburg, Germany) and cultured in complete RPMI medium, allow the measurement by flow cytometry of the main CAR-mediated activation signaling pathways (NFAT, NFkB and AP1 pathways) after antigen recognition.[15] The PM299L-Thy1.1 and PM299L-EDA cell lines were generated by retroviral transduction of PM299L-WT cells with a retrovirus expressing EDA fused to the transmembrane domain of PDGFR and the membrane cell marker Thy1.1 (RV-EDA-PDGFR-IRES-Thy1.1 plasmid). A cell line expressing only the Thy1.1 cell marker was also generated. Two different PM299L-EDA cell clones were isolated to express low (PM299L-EDA^low) and high (PM299L-EDA^high) levels of EDA on the cell membrane. The Platinum Ecotropic (Plat-E, ATCC) and HEK293T cell lines were cultured in DMEM supplemented with 10% FCS and the selection antibiotics puromycin (100 µg/mL) and blasticidin (10 µg/mL). All cell lines were cultured at 37°C in a humidified atmosphere with 6.5% CO_2.

Expression and purification of anti-EDA scFv (F8)
A DNA sequence coding for the scFv recombinant antibody fragment F8[16] was cloned in pET20b plasmid (Novagen), which enables expression of fusion proteins carrying six histidine residues at the carboxyl terminus. The resulting plasmid was transfected into BL21(DE3) cells for the expression of the recombinant scFv which was purified by affinity chromatography using protein

A Sepharose (Amersham Biosciences) according to the manufacturer's instructions. Purified antibody fragments were analyzed by Coomassie and Western blot using anti-His antibodies. Recognition of EDA protein by the purified scFv F8 fragment was tested by ELISA using plates coated with recombinant human and mouse EDA proteins produced as described previously.[17] The equilibrium dissociation constant (K_D) of scFv F8 to soluble human and mouse EDAs was calculated by bio-layer interferometry (BLI) using an Octet N1 (Sartorius) (online supplemental figure 1). The scFv F8 was coated to the AR2G Biosensors (Fortébio) following manufacturer's instructions.

Viral vectors and virus production

The chimeric EDA CAR used to generate the murine CAR T cells is composed of the anti-EDA F8 scFv and a murine 4-1BB-CD3ζ expression cassette linked through a F2A self-cleaving peptide sequence to eGFP. The PSMA CAR, used as an irrelevant CAR, included the anti-human PSMA scFv obtained from mouse hybridoma J591, that was cloned in the same expression cassette. For selected experiments the chimeric EDA CAR expression cassette was linked to luciferase expressing gene. The EDA CAR used to produce human CAR-T cells also contained the anti-EDA F8 scFv and the human endodomains 4-1BB-CD3ζ. This cassette was cloned in a third-generation self-inactivating lentiviral vector (LV) and regulated under an EF1α promoter. To facilitate the quantification of the transduction, LV EDA CAR also included the blue fluorescent protein reporter gene. These plasmids were synthesized by Genscript.

For retrovirus productions, Plat-E cells were transfected with 5 µg of retroviral plasmid DNA along with 2.5 µg pCL-Eco plasmid DNA using lipofectamine 2000 (Invitrogen) for 6 hours in antibiotic-free medium. Retroviral supernatants were collected at 48 and 72 hours after transfection.

For lentivirus production, replication-defective LVs were produced in HEK293T cells. Briefly, 6×10^6 cells were plated in p100 culture dishes and 24 hours later were cotransfected with 6.9 µg of the CAR expressing plasmid, 3.41 µg pMDLg/pRRE (Gag/Pol), 1.7 µg pRSVRev and 2 µg pMD2.G (VSVG envelope) packaging plasmid using lipofectamine 2000. Forty hours after transfection, supernatants were collected, filtered and concentrated using the Lenti-X Concentrator (Takara) following the manufacturer's specifications.

Car T cell generation

Murine CAR-T: purified murine $CD4^+$ and $CD8^+$ T cells were activated with dynabeads CD3/CD28 at a 1:2 bead:T cell ratio for 24 hours in RPMI complete media containing 100 IU/mL recombinant human interleukin-2 (rhIL-2). Twenty-four hours later, T cells were infected with the retrovirus expressing the CAR and incubated with 100 IU/mL rhIL-2 and 10 µg/mL protamine sulfate (Sigma) and spun at 2000xg at 32°C for 90 min. Infection was repeated 1 day later. After infection, lymphocytes were cultured in complete RPMI medium with IL-2 until day 5 and used for functional in vitro or in vivo assays.

Human CAR-T: $CD4^+$ and $CD8^+$ cells were isolated from PBMCs using CD4 and CD8 MicroBeads (Miltenyi Biotec) in the AutoMACS Pro Separator (Miltenyi Biotec). Isolated T cells were activated with 10 µl/mL T cell TransAct (Miltenyi Biotec) for 48 hours and infected with the CAR LV at MOI 3 with 10 µL/mL of Lenti-Boost (Sirion Biotech). CAR-T cells were expanded in RPMI 1640 culture medium supplemented with 3% human serum (Sigma), 1% penicillin/streptomycin, and 625 IU/mL of human IL-7 and 85 IU/mL of human IL-15 (Miltenyi Biotec). CAR-T cells were counted, and the concentration was adjusted to 1×10^6 cells/mL every 2 days. Transduction efficiency was evaluated by FACS measuring reporter gene expression. Untransduced cells used as controls in some experiments were prepared following the same protocol used for CAR-T cell preparation but without viral transduction.

Antibodies and flow cytometry

Samples were tested with a FACS Canto II flow cytometer (Becton Dickinson) and data were analyzed by FlowJo software (TreeStar). EDA and control PSMA CARs were detected by the expression of GFP and/or by using Biotin-SP-conjugated anti-human or anti-mouse immunoglobulin G antibodies (109-066-097 and 115-066-072 respectively, Jackson Immunoresearch), followed by incubation with fluorochrome-conjugated Streptavidin (Biolegend).

The transduced PM299L-WT cells (PM299L-EDA or PM299L-Thy1.1) were sorted by using an anti-Thy1.1 antibody (OX-7, Biolegend). EDA expression in tumor cell lines was tested though flow cytometry with anti-EDA scFv (F8) antibody followed by a fluorochrome-conjugated anti-6x-His Tag antibody.

T-cell phenotype was assessed by using the following fluorochrome-conjugated antibodies (Biolegend) at 0.25–1 µg/mL: CD8a (53–6.7), CD4, (RM4-5) CD45.1 (A20), CD45.2 (104), CD44 (IM7), CD62L (MEL-14), CD137 (17B5), PD1 (29F.1A12), TIGIT (1G9) and LAG3 (C9B7W). For staining, cells were incubated with the Zombie NIR Fixable Viability kit (Biolegend) for 15 min at room temperature and then washed once with washing buffer. Cells were fixed and permeabilized with the Foxp3/Transcription Factor Staining kit buffers (eBioscence) and then stained intracellularly (15 min, RT) with fluorochrome-conjugated mAbs against mouse, Ki67 (16A8), TNF-α (MP6-XT22) and IFN-γ (XMG1.2). Perfect-Count beads (Cytognos) were added for the flow cytometry quantification of absolute cell numbers.

Immunohistochemistry

For immunohistochemichal detection of EDA, α-SMA, CD31 or collagen IV in paraffin embedded tumor tissue sections, antigen retrieval was performed by heating the samples in a microwave oven using citrate buffer (10 mM, pH 9 for EDA, and pH 6 for CD31 and collagen IV). After

blocking non-specific binding sites, the primary antibody scFv F8 was added and incubated at 5 µg/mL overnight at 4°C. When indicated, the anti-EDA antibody used was IST-9 (sc-59826, Santa Cruz) at the same concentration. After washing with TBS solution, slides were incubated with the anti-6x-His Tag antibody (RM146, Abcam) at a 1:200 dilution for 45 min at room temperature. After TBS washes, samples were incubated with Dako EnVision+System HRP Labeled Polymer Anti-Rabbit during 30 min at room temperature. For quantification, slides were scanned with the Aperio CS2 scanner (Leica, Barcelona, Spain) and images were visualized with the Aperio Image Scope (V.12.1.05029). Slides were scanned with the Aperio CS2 scanner (Leica, Barcelona, Spain) and images were visualized with the Aperio Image Scope (V.12.1.05029). For quantification, 10 non-overlapping fields were randomly selected from each tissue preparation, and optical density (DAB chromogen signal corresponding to EDA protein expression) was calculated in all tissue slides using ImageJ software using the Color Deconvolution plugin. In human tumor samples, the obtained signal was compared with that corresponding to each healthy tissue stained with the scFv F8. The rest of the samples were compared with the negative control consisting of the same slide only stained with the secondary antibody.

Multiplexed immunohistochemistry
Paraffin-embedded tissue sections were used for multiplexed immunofluorescence microscopy using these combinations of antibodies: anti-EDA scFv F8 antibody and anti-human CD31 (77699S, Cell Signaling) and; anti-EDA scFv F8 and Collagen IV (ab6586, Abcam). Samples were stained using an Opal 4-color anti Rabbit Kit (NEL840001KT, Akoya Biosciences) following manufacturer's instructions. Samples were counterstained using DAPI and digitalized using a PhenoImager HT scanner (Akoya Biosciences).

Characterization of CAR-T cells
Car expression on surface and binding to EDA protein
The CAR expression was measured by flow cytometry, 1×10^5 EDA or PMSA CAR-T cells were incubated with biotinylated anti-human or anti mouse IgG, respectively, at 1 µg/mL of (Jackon ImmunoReseach) for 40 min at 37°C. After washing, cells were stained with APC conjugated-Streptavidin for 15 min at room temperature.

To evaluate the capacity of the EDA CAR-T cells to bind EDA, cells were incubated with murine and human recombinant EDA proteins at 5 µg/mL. After 20 min of incubation with the protein at 37°C, cells were washed and labeled with the anti-HIS tag AF647 antibody during 15 min at room temperature and analyzed by flow cytometry.

Car-T cell response to EDA
5×10^5 CAR-T cells were plated in 96-well plates pre-coated with recombinant EDA or recombinant ovalbumin OVA (Endograde) as an irrelevant protein for 48 hours. CAR-T cell proliferation and IFN-γ production after recombinant EDA stimulation were measured by 3H-thymidine incorporation (0.5 µCi per well) and ELISA, respectively, as described.[18]

Also, CAR-T cells were plated for 24 hours in the presence of irradiated PM299L-EDA^high^ and PM299L-Thy1.1 cells. The number of IFN-γ producing cells was measured by ELISPOT as described.[19] In some cases, CAR-T cell proliferation was measured by Cell trace violet (CTV) dilution assay; lymphocytes were incubated with the dye (5 µM) for 15 min at 37°C and washed with RPMI 10%FBS. 8×10^5 labeled lymphocytes were plated and co-incubated with PM299L-EDA^high^ and PM299L-Thy1.1 tumor cells at a ratio of 1:1 for 72 hours at 37°C. Subsequently, the proliferating population (measured by CTV dilution) was analyzed within GFP$^+$ lymphocytes. The proliferation index was calculated as the ratio between proliferating cells in the presence of tumor cells expressing EDA (PM299L-EDA^high^ or the control PM299L-Thy1.1) and the number of proliferating cells in the condition without stimulation at the end of the co-culture.

Cytotoxicity assays
Real-time cytotoxicity assay (xCELLigence) was carried out to analyze the cytotoxicity of the CD8$^+$ CAR-T cells as previously described[19] and using an Effector:Tumor cell ratio of 1:1). All experiments were performed in duplicate.

CAR-T cell cytotoxicity was also measured by flow cytometry. 6×10^5 CAR-T cells were cocultured with PM299L-EDA^high^ PM299L-EDA^low^ or PM299L-Thy1.1 cells for 24 hours at two different Effector:Tumor ratios (1:1 and 0.2:1). Then, cells were washed and incubated with a fluorochrome-conjugated antibody against CD8. PerfectCount beads (Cytognos) were added for the flow cytometric quantification of absolute cell numbers.

In vivo assessment of anti-EDA CAR-T cell antitumor activity
Winn assay. C57BL/6 mice (8–10 weeks of age) were sublethally irradiated (total body irradiation) with 4 Gy. Then, mice were injected with 2×10^6 PM299L-EDA^high^ cells by the subcutaneous (s.c.) route and received 2×10^6 CD4$^+$ and 6×10^{106} CD8$^+$ CAR-T cells by the intravenous route.

PM299L-EDA established tumor. C57BL/6 female mice (8–10 weeks of age) were injected with 2×10^6 PM299L-EDA^high^ cells by the s.c route. Seven days later, mice were irradiated with 4 Gy and received 9×10^6 CAR-T cells.

F9 established tumor: 129Sv mice (8–10 weeks of age) were injected with 3×10^6 F9 cells by the s.c route. Seven days later, mice were irradiated and received 1×10^7 CAR-T cells (CD4 and CD8 ratio 5:1).

All mice received also 20.000U human IL2/day during 4 days after T cell infusion.

Xenograft mouse model: The 8–10 weeks old male/female NOD scid gamma (NSG) mice obtained from the CIMA NSG colony were injected s.c. with 3×10^6 PLC tumor cells embedded in Matrigel (Corning; 1:1 diluted in PBS). On day 8 after tumor injection, when tumors

were 5–7 mm in diameter, mice received a single intravenous dose of 5×10^6 untransduced T cells, EDA CAR-T cells, or were left untreated.

In all these models, tumor area was monitored with a caliper every 2–3 days after T cell infusion. Mice were sacrificed when tumor diameter reached a value >2 cm. There were no exclusion of animals in the analyses.

In vivo imaging

For Angiosense imaging, mice-bearing F9 tumors were injected with a single intravenous dose of angiosense 750 (2 nmol/100 µL) as recommended by the manufacturer (NEV10011EX, PerkinElmer). After 24 hours of Angiosense 750 administration, fluorescence accumulation into the tumor was visualized using the PhotonImager Optima (Biospace, Paris, France). Relative fluorescent units were calculated by measuring tumor fluorescence divided by tumor volume. For luciferase imaging, and to evaluate CAR-T cell persistence and expansion in vivo, C57BL/6J mice were injected intravenously with 1×107 EDA CAR-T luciferase or PSMA CAR-T luciferase. Luciferase activity was measured 10 min after intraperitoneal injection of 3 mg/mouse of the substrate D-luciferin (Thermo Fisher Scientific), on days 1, 3, 7, 10 and 14 postinfusion with the PhotonIMAGER Optima and the M3Vision Analysis software (Biospace Lab, France).

Rnaseq analysis

Total RNA from tumors was isolated using the MagMAX mirVana total RNA isolation Kit (Applied Biosystems). Following mechanical homogenization with an Ultra-turrax (T10 basis Ultra-Turrax, IKA), RNA was extracted according to the manufacturer's instructions and stored at −80°C until processed. RNA concentration was quantified using a Qubit V.3.0 Fluorometer and its quality was examined in Agilent's 4200 TapeStation System. Roughly 150 ng of quality total RNA were used for the transcriptome interrogation using the Illumina Stranded Total RNA Prep Ligation with Ribo-Zero Plus kit according to the manufacturer's instructions (Illumina). Briefly, cytoplasmic and mitochondrial rRNAs as well as beta globin transcripts were depleted from the samples. The remaining RNA was fragmented and reverse-transcribed. A second strand cDNA synthesis step removed the RNA template while incorporating dUTP in place of dTTP in order to preserve strand specificity. Next, double-stranded cDNA was A-tailed, then ligated to Illumina anchors bearing T-overhangs. PCR-amplification of the library allowed the barcoding of the samples with 10 bp dual indexes and the completion of Illumina sequences for cluster generation. Libraries were quantified with Qubit dsDNA HS Assay Kit and their profile was examined using Agilent's HS D1000 ScreenTape Assay. Sequencing was carried out in an Illumina NextSeq2000 using paired-end, dual-index sequencing (Rd1: 59 cycles; i7: 10 cycles; i5: 10 cycles Rd2:59 cycles) at a depth of 50 million reads/sample.

RNA-seq reads are trimmed using Trim Galore V.0.4.4 using default parameters to remove the Nextera adapter sequence. Mapping is performed using STAR (2.6) against the mouse NCBIM37 genome, guided by gene models from Ensembl annotation release 68. Quantification and generation of gene expression matrices were performed with the function featureCounts, implemented in the R package Rsubread. Aligned fragments are imported into RStudio and before statistical analysis, the function filterbyExpr, implemented in the R package edgeR, was used to determine genes with enough counts for further analyses. Differential gene expression analysis is performed using the DESeq2 algorithm within R and RStudio. Gene set enrichment analysis was carried out using GSEA software (https://www.gsea-msigdb.org/).

Safety study

Naïve C57BL/6J mice were were sublethally irradiated and received 1×10^7 CAR-T cells (5×10^6 CD8 and 5×10^6 CD4). Blood samples were obtained at day 17 and 30 after CAR-T cell infusion and mice were sacrificed and tissues were collected at day 30. Serum biochemical parameters were measured by a Roche Cobas 6000 analyzer (Roche Diagnostics, Mannheim, Germany). Liver, spleen, lung, kidney and heart were also resected from the mice and stained with hematoxylin and eosin (H&E) for toxicity evaluation.

Ex vivo analysis of tumor-infiltrating T cells

PM-299L-EDA^{high} or F9 tumors were harvested between days 4–9 after T cell injection. Excised tumors were digested with 400 U/mL collagenase-D and 50 µg/mL DNase-I (Roche) for 20 min at 37°C. For functional analyses, cells were stimulated with PMA (50 ng/mL)/Ionomycin (1 µg/mL) and GolgiStop/GolgiPlug (BD Biosciences). After 5 hour, cells were incubated with Zombie NIR Fixable dye (Biolegend). Subsequently, they were stained with fluorochrome-conjugated mAbs against CD45.2 (104), CD8 (XMG1.4), PD1 (29F.1A12), LAG3 (C9B7W), and TIGIT (1G9) in the presence of purified anti-CD16/32 mAb. For intracellular staining, cells were fixed and permeabilized with the BD Fixation/Perm buffer (BD Biosciences) and stained with anti-IFN-γ (XMG1.2) and with anti-KI67 (16A8) mAbs.

For human tumor-infiltrating T cells studies, PLC tumor were harvested at day 7 after T cell infusion and manipulated as described above for murine experiments. The tumor cell suspension was stained with anti-CD3 (UCHT1), anti-ICOS (G398.4A), anti-CD137 (4B4-1), anti-PD1 (EH12.2H7), anti-LAG3 (TA7530) and anti-TIGIT (A15153G). After fixation and permeabilization, cells were stained with anti-GzmB (QA16A02). Samples were acquired on a FACSCanto-II cytometer (BD Biosciences). Data were analyzed using FlowJo software (TreeStar).

Statistical analysis

Normality was assessed with Shapiro-Wilk W test. Statistical analyses were performed using parametric Student's t-test, two-tailed paired t-tests, and one-way ANOVA (Analysis of Variance) with the Bonferroni multiple comparison test, as indicated. The Mann-Whitney U and Kruskal-Wallis tests were used for non-parametric analyses. For all tests, a $p < 0.05$ was considered statistically significant. Descriptive data for continuous variables were reported as means±SD. GraphPad Prism V.7 (GraphPad Software) was used for statistical analysis.

RESULTS

EDA is expressed in human tumor samples

We analyzed the EDA fibronectin (FN1) mRNA splicing pattern in a panel of 15 different tumors using The Cancer Genome Atlas (TCGA) RNASeq data and the TCGA SpliceSeq resource (http://projects.insilico.us.com/TCGASpliceSeq) (figure 1A). This analysis highlighted the upregulation of EDA in human cholangiocarcinomas (CHOL), breast cancer (BRCA), head and neck squamous cell carcinoma (HNSC) and in liver cancer (LIHC), with respect to the EDA expression in the corresponding adjacent normal tissues. We also found significant differences in colon adenocarcinoma, kidney renal clear cell carcinoma, lung adenocarcinoma, lung squamous cell carcinoma, prostate adenocarcinoma or uterine corpus endometrial carcinoma. However, in these cases, the differences in mean between the tumor and the normal tissue was lower than 10%, as opposed to the strong differences (>25%) found for CHOL, BRCA, HNSC or LIHC (highlighted in color). We confirmed the results obtained from the TCGA data base in a cohort of 17 patients with hepatocarcinoma with available RNASeq data from our institution. HCC tumor samples had a very significant increase in EDA expression in tumor tissues compared with the corresponding adjacent non-tumoral tissue (figure 1B).

We then measured the EDA expression in different tumors at the protein level using the human antibody fragment scFv (F8) specific for the EDA domain.[16] These analyses confirmed and expanded the results previously reported by Rybak et al.[16] As compared with the corresponding healthy tissue, we found strong EDA expression in human biopsies of cholangiocarcinoma, hepatocarcinoma, colon, ovarian and pancreatic cancers, whereas these differences were mild in other gastrointestinal cancers (colon, duodenal and stomach cancers) (figure 1C). EDA expression compared with the corresponding healthy tissue controls was quantified using ImageJ software (figure 1D).

We also measured the EDA expression in tumor tissues induced in NSG mice after subcutaneous injection of human hepatocarcinoma (PLC and HUH7) and cholangiocarcinoma (HuCCT and TFK1) cell lines (figure 1E). In agreement with the results found in human tumor biopsies, prominent staining of tumor stroma and the

neovasculature within the tumor was observed in both types of tumors. EDA/CD31 colocalization experiments in tumor samples from these NSG mice challenged with PLC, HUH7, HUCCT and TFK1 human tumor cell lines, showed in all cases a broad EDA staining of tumor stroma and also in the basement membrane of the tumor neovasculature, close to CD31 staining. These images suggest that EDA is expressed in the ECM surrounding and supporting the endothelial cells but not in the endothelial cells themselves (figure 1F). Since type IV collagen is the main component of the basement membrane and it plays a role in endothelial cell proliferation[20] we carried out also collagen IV-EDA colocalization experiments in PLC and F9 tumors. As control we included tissue sections from healthy murine kidney. It was found an important but not exclusive colocalization of EDA and type IV collagen in F9 and PLC tumors whereas no EDA expression was detected in the normal kidney (online supplemental figure 2A).

It has been described that cellular fibronectin is synthesized by many cell types, including fibroblasts, endothelial cells, myocytes or tumor cells. To find out the origin of the EDA protein detected in human tumors induced in NSG mice, we used two different anti-EDA antibodies: the IST-9 antibody that only detects the human protein and the scFv F8 that detects both the human and murine EDA protein. It was observed that in the case of the hepatocarcinoma tumors studied (PLC and HUH7), the EDA deposited in the ECM and around the endothelium was human and thus must be produced by the human tumor cells. However, in the case of the TFK1 cholangiocarcinoma tumor, unlike the HUCCT, the origin is from mouse cells, possibly macrophages, fibroblasts, or endothelial cells. We included the staining of human hepatocarcinoma and human cholangiocarcinoma biopsies to check the staining pattern of both antibodies (online supplemental figure 2B).

### EDA expression in murine tumor cell lines and tumor tissues

Since F8 scFv engages human and mouse EDA protein (96.6% homology), we also measured by flow cytometry the EDA expression in different tumor murine cell lines (B16OVA melanoma, LLCOVA lung carcinoma and F9 teratocarcinoma) cultured in vitro. We found a marginal staining in the LLCOVA cell line, which is upregulated when cells are cultured for 16 hours in the presence of TGF-β, a well described inducer of EDA splicing[21 22] (online supplemental figure 3A). EDA expression was then analyzed in tumor tissues induced in mice after subcutaneous injection of the indicated cell lines. We found some positive staining for EDA in F9 tumors. However, no expression was detected in LLCOVA or in B16OVA induced tumors. As previously described for F9 tumors,[16] EDA staining was mainly located in endothelial cells (online supplemental figure 3B).

EDA CAR-T cells recognize EDA and kill EDA expressing tumor cells

We prepared a retroviral construct encoding a cassette for the expression of EDA-specific CAR cloned in the
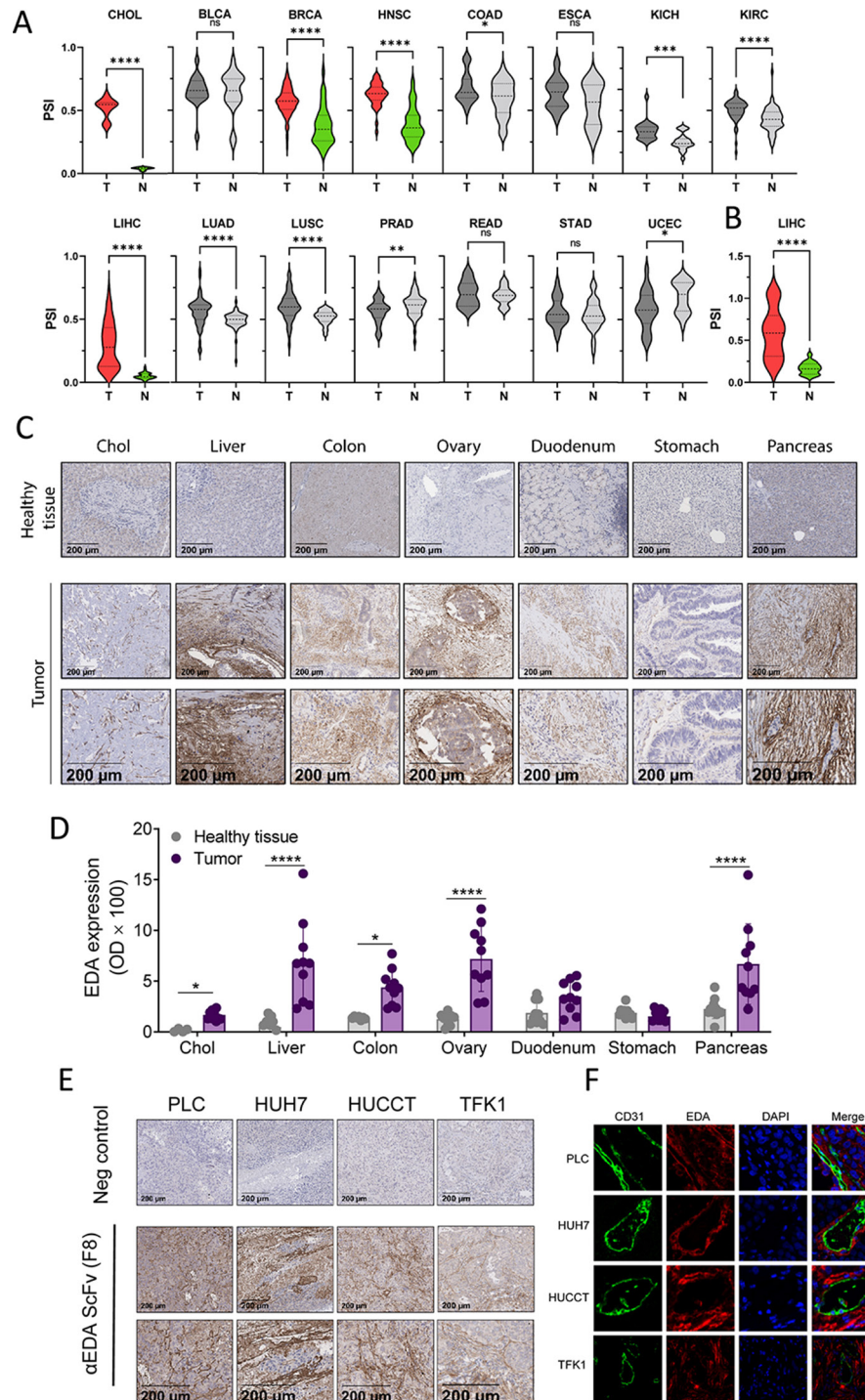
Figure 1 Extra domain A (EDA) expression on tumor tissues (A, B) percentage of spliced fibronectin in several types of human tumor samples compared with corresponding adjacent healthy tissue. RNAseq analysis from TCGASpliceSeq data set (A) or from a cohort of patients with hepatocarcinoma (B). EDA expression in tumor samples (red bars) and in healthy tissue (green bars) is plotted in color when differences in mean were >25%. (C, D, E) Immunohistochemical detection of EDA in tumor biopsies from different cancer patients and the corresponding healthy tissue as control (C) and from tumor biopsies from NSG mice xenografted with human hepatocarcinoma or cholangiocarcinoma cell lines. (E). (D) Quantification of EDA expression in the indicated tumor samples and healthy tissues measured by using ImageJ software. (F) confocal immunofluorescence analysis of the expression of CD31 and EDA in PLC, Huh7, HUCCT and TFK1 tumor samples obtained from NSG mice. *P<0.05, **P<0.01, ***P<0.005, ****p<0.001. paired t-test (A). Student t-test (D). bars representing the mean and SD are plotted. PSI, per cent-spliced-in value.
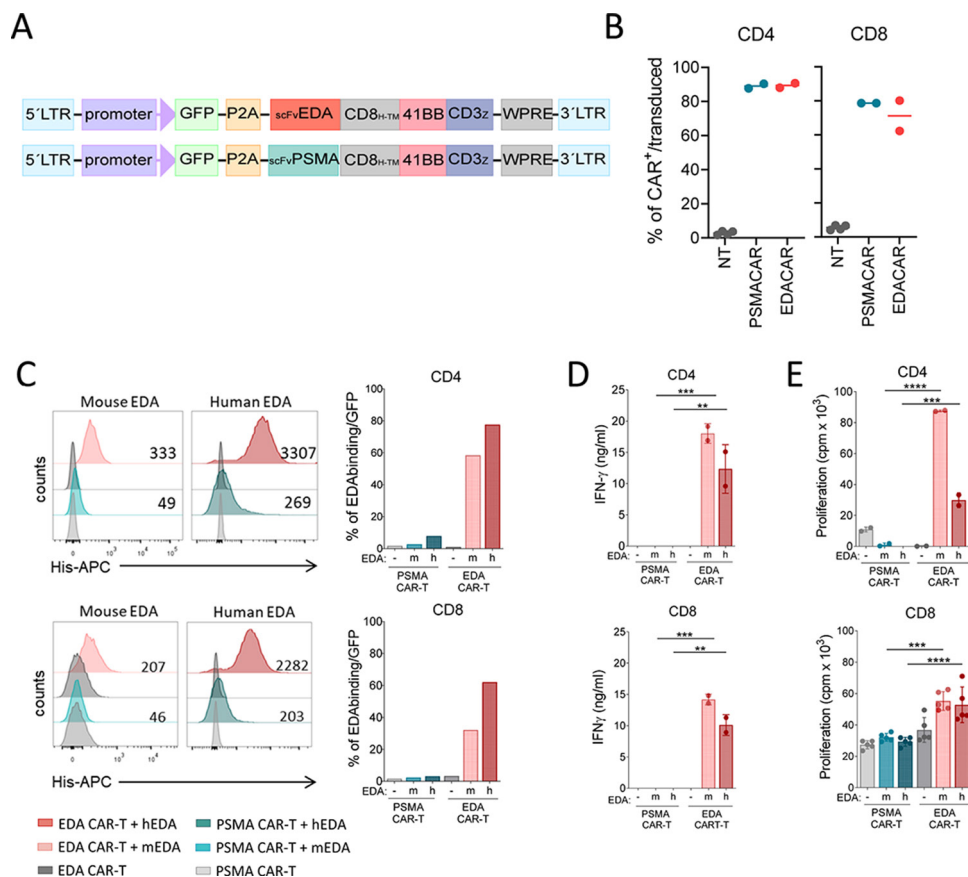
Figure 2 Generation and in vitro characterization of EDA CAR-T cells. (A) scheme representing the second generation EDA CAR and control PSMA CAR structures. (B) CAR expression measured by staining with anti-idiotype antibody specific for human IgG (H+L) for EDA CAR-T and anti-mouse for PSMA CAR-T on the surface of transduced T cell, both CD4 (left) and CD8 (right). (C) EDA ligand binding assay for EDA CAR-T (red histogram) or control PSMA CAR-T (blue histogram). CD4+ or CD8+ CAR-T cells were incubated with recombinant human and mouse His-EDA protein (50 µg/mL) and stained with anti His-APC antibody. numbers in histograms indicate mean fluorescence intensity. (D–E) CAR-T function after antigen-specific stimulation. (D) IFN-γ production by EDA CAR-T or PSMA CAR-T cells after 48 hours of stimulation with mouse EDA (m) or human EDA (h) protein coated plates at 5 µg/mL. (E) CD4+ or CD8+ CAR-T cell proliferation in response to EDA measured by 3H-Timidine incorporation. Data are representative of three independently repeated experiments. **P<0.01, ***p<0.005, ****p<0.001. One-way ANOVA with Bonferroni multiple comparisons test (D, E). bars representing the mean and SD are plotted. CAR-T, chimeric antigen receptor T-cell; EDA, extra domain A. PSMA, prostate-specific membrane antigen; ANOVA, Analisis of Variance.

pRubiG plasmid in frame with the eGFP-P2A gene to express eGFP and the CAR simultaneously. As a control we also prepared a pRubiG plasmid expressing an anti-PSMA CAR (figure 2A). EDA and PSMA CAR-T cells were generated by retroviral transduction of CD4+ or CD8+ T cells with the corresponding retrovirus. Five days after infection, T cells were analyzed by flow cytometry. Both CD4+ and CD8+ PSMA CAR-T and EDA CAR-T transduced cells express their respective CAR construct with an efficiency of transduction in the 80% range in both cases (figure 2B). Both CD4+ and CD8+ EDA CAR-T but not PSMA CAR-T cells were able to interact with both human and mouse recombinant EDA proteins, demonstrating the specificity of the EDA CAR (figure 2C).

To evaluate the functionality of the CAR construct, EDA CAR-T cells were cultured in EDA coated plates for 48 hours. Both CD4+ and CD8+ EDA CAR-T, but not PSMA CAR-T cells produced high amounts of IFN-γ (figure 2D) and proliferated in response to EDA

(figure 2E). Curiously, there was an apparent inverse correlation between EDA binding capacity (figure 2C) and functional responses by EDA CAR-T cells to mouse and human EDAs (figure 2D,E). This discrepancy could be due to the methodological differences between assays. Indeed, in the binding experiments EDA proteins are added in solution and bind to the CAR-T cells directly. However, in the functional experiments (IFN-γ production or CAR-T cell proliferation), the EDA proteins are coated into the plate to allow the CAR crosslinking. Using BLI assays, we found that although scFv F8 binds with similar KD for both proteins in solution, the human EDA is recognized with a slightly higher affinity than the murine EDA (7.763×10^{-8} M vs 9.954×10^{-8} M, respectively). However, scFv F8 recognizes better to murine EDA protein when it is coated to ELISA plates (online supplemental figure 1). These findings might explain why the EDA CAR-T cells bind better the human EDA when it is

in solution (figure 2C) whereas they produce more IFN-γ in response to murine EDA when it is coated in plastic plates (figure 2D,E).

To study the capacity of EDA CAR-T cells to recognize tumor cells expressing EDA, we used the PM299L HCC cell clones PM299L-EDA^{low} and PM299L-EDA^{high}, expressing different levels of EDA on the cell membrane (online supplemental figure 4AB). EDA CAR-T cells produced high levels of IFN-γ in response to the different PM299L cells clones. As expected, PM299L-EDA^{high}, which express high levels of the antigen, stimulated the secretion of higher levels of IFN-γ by both CD4$^+$ and CD8$^+$ EDA CAR-T cells than those induced by clone PM299L-EDA^{low}. Control PSMA CAR-T cells did not react against these cell lines indicating the specificity of EDA recognition only by EDA CAR-T cells (figure 3A,B). T cell proliferation, CD69 expression and the production of IL-2 and IFN-γ cytokines by CD4 or CD8 EDA CAR-T cells in response to stimulation with PM299L-EDA^{high}, indicated that EDA CAR is antigen specific and efficiently triggers T cell activation (figure 3C).

The tumor killing capacity of EDA CAR-T cells against the different EDA-expressing PM299L clones was measured by flow cytometry. EDA CAR-T cells lysed with higher efficiency the PM299L-EDA^{high} than the clone PM299L-EDA^{low}. However, PSMA CAR-T cells did not recognize these cell clones (figure 3D). Similar results were found in the real-time cytotoxicity assay (xCELLigence) (figure 3E). The PM299L-Thy1.1 cell line, which does not express EDA, was used as control. Percentage of cell lysis was proportional to the level of EDA expression by PM299L cells.

EDA CAR-T cells exerts antitumor activity in different murine tumor models

To evaluate the antitumor activity of EDA CAR-T cells we used different murine tumor models. First, the antitumor activity of EDA CAR-T cells was tested in a Winn-type assay[23] where C57BL/6 mice were challenged subcutaneously with $2.5×10^6$ PM299L-EDA^{high} cells expressing high levels of EDA in vitro and in vivo (online supplemental figure 4B,C, respectively) and treated intravenously at the same time with $2.5×10^6$ CD4$^+$ and $6×10^6$ CD8$^+$ EDA CAR-T or PSMA CAR-T cells. While all mice treated with PSMA CAR-T cells developed tumors, administration of EDA CAR-T cells led to complete rejection of injected tumor cells and all animals survived to tumor challenge (figure 4A, left panel). These surviving EDA CAR-T cell treated mice were rechallenged at day 40 with PM299L-EDA^{high} tumor cells and blood samples were obtained at different time points to evaluate EDA CAR-T cell expansion by flow cytometry. We found a clear CAR-T cell expansion 5 days after tumor rechallenge. The EDA CAR-T numbers dropped to basal levels at day 20 after this rechallenge (figure 4A, right panel). All mice remained tumor free and no signs of toxicity were observed. These results suggest the establishment of a long-lasting immunity that might protect mice from metastatic recurrence.

Second, C57BL/6 mice where challenged with PM299L-EDA^{high} cells ($2.5×10^6$ cells) expressing high levels of EDA in vitro and in vivo. Seven days later, when tumors were palpable, the mice were treated with a mixture of $7×10^6$ CD4$^+$ and $2×10^6$ CD8$^+$ EDA CAR-T or PSMA CAR-T cells. All mice treated with EDA CAR-T, but not with PSMA CAR-T cells, rejected the tumor (figure 4B and online supplemental figure 5).

Four days after T cell therapy, mice treated with EDA CAR-T showed a significantly higher number of intratumoral CAR-T cells, with a higher level of activation (measured as the percentage of CD4$^+$ or CD8$^+$ CD137$^+$ cells), but also a higher percentage of PD1$^+$ TIGIT$^+$ T cells than those treated with PSMA CAR-T (figure 4C). Characterization of the functionality of CAR-T cells present in the spleen also showed a higher percentage of proliferating (Ki67$^+$ IFN-γ$^+$) CD4$^+$ and CD8$^+$ EDA CAR-T in response to EDA stimulation (figure 4D).

We evaluated the migratory capacity of CAR-T cells to the site of antigen expression in mice-bearing the EDA expressing PM299L-EDA^{high} (injected into the right flank) and the original PM299L tumor cell line (EDA negative) (injected into the left flank). CD4$^+$ and CD8$^+$ EDA CAR-T or PSMA CAR-T cells were injected intravenously and 7 days after infusion, both tumors were excised to analyze the number of CAR-T cells in each one. Notably, we found that EDA CAR-T cells were enriched in the PM299L-EDA^{high} tumor as compared with that found in the PM299L (measured as the number of CAR-T cells/mg of tumor). There was also an increase in the percentage of CAR-T cells expressing PD1 within the EDA-expressing tumor. However, PSMA CAR-T cells poorly infiltrated the tumors and showed no preference for any of them (figure 4E).

We then wanted to evaluate the antitumor capacity of EDA CAR-T cells in a tumor not forced to express EDA by genetic modification. Among B16OVA, LLCOVA or F9 induced tumors only the F9 teratocarcinoma tumor model expressed detectable levels of EDA (online supplemental figure 3B). In this F9 cell-based tumor model, Rybak et al[16] described that the cells expressing EDA are the endogenous endothelial cells and not the tumor cells. To confirm this findings, we carried out CD31 and EDA colocalization experiments in F9 tumors as well as in B16OVA. Interestingly, EDA expression colocalized with CD31 in F9 tumors, however, we could not detect EDA in B16 tumors, not in the tumor stroma nor in the tumor vasculature (online supplemental figure 3C). Then, we tested the antitumor efficacy of EDA CAR-T in animals bearing F9 teratocarcinoma. 129Sv mice were challenged with F9 tumor cells ($3×10^6$ cells injected subcutaneously). When tumors were palpable, mice were treated with EDA CAR-T or PSMA CAR-T cells (a mixture of $1×10^7$ CD4$^+$ and CD8$^+$ CAR-T cells). It was observed that, although tumors were not totally controlled, administration of EDA CAR-T cells was able to significantly delay tumor growth (figure 5A). Characterization of CAR-T cells in F9 tumor-bearing mice, 7 days after cell transfer, indicated
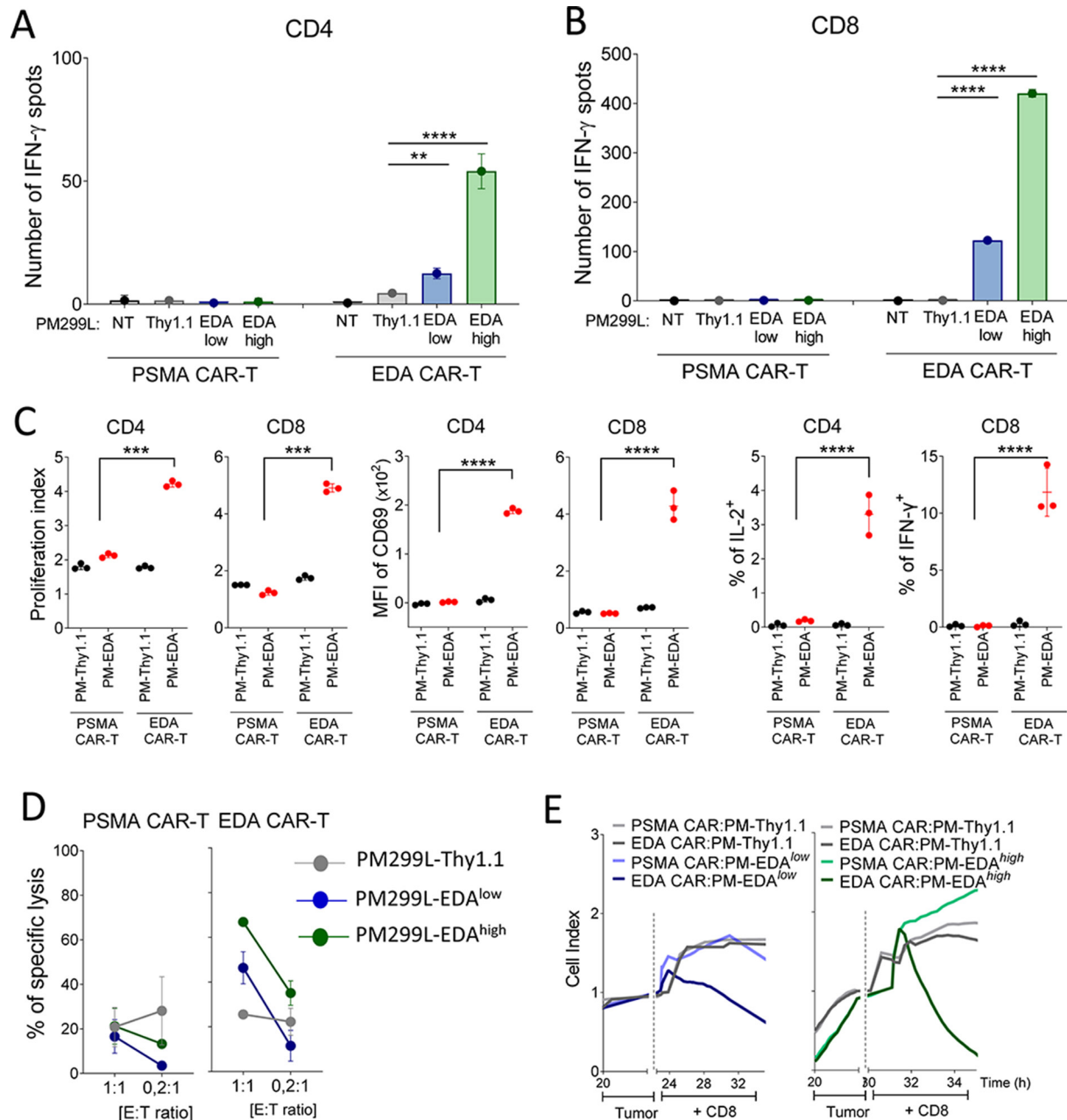
Figure 3 EDA CAR-T cells recognize EDA-expressing tumors. (A–B) Number of IFN-γ producing cells in response to PM299L-EDA^high and PM299L-EDA^low clones. CD4 (A) and CD8 (B) CAR-T cell were stimulated for 24 hours with PM299L expressing high or low levels of EDA on their membrane or with wild type PM299L-Thy1.1 cell lines at 1:1 ratio. (C) CAR-T cell proliferation rate, CD69 expression, IL-2 and IFN-γ production in response to stimulation with PM299L-EDA^high or with PM299L-Thy1.1 were measured by flow cytometry. (D) lytic activity of CAR-T cells. lysis of PM299L-EDA^high, PM299L-EDA^low or EDA^- (PM299L-Thy1.1) tumor target cells measured by flow cytometry after 24 hours of cell cocultures (1:1 or 0,2:1 CAR-T: target cell ratio). (E) Real-time cytotoxicity measured by xCELLigence. *P<0.05, **p<0.01, ****p<0.001. One-way ANOVA with Bonferroni multiple comparisons test (A, B, C). Bars representing the mean and SD are plotted. Clones PM299L-eda^high express high levels of EDA. PM299L-eda^low: express low levels of EDA. PM299L-Thy.1.1: EDA negative cell line used as a control. CAR-T, chimeric antigen receptor T-cell; EDA, extra domain A; NT, no stimulated

a slightly higher percentage of PD1^+ cells in CD8 EDA CAR infiltrating the tumor with respect to PSMA CAR-T cells, although this difference was not statistically significant for CD4 EDA CAR-T cells (figure 5B). Mice treated with EDA CAR-T cells also had a higher percentage of IFN-γproducing CD4 or CD8 CAR-T cells in the draining lymph nodes and in the spleen (figure 5C,D respectively).

We observed a certain degree of endogenous CD8 T cells producing IFN-γ also in the PSMA CAR-T cells treated mice. This increase could be related to the in vivo treatment with IL-2. Regarding the tumor infiltrating leukocytes infiltration at day 14 after CAR-T infusion, we found a significant increase in the percentage of CD11b^+ cells, in particular the Ly6G^+ Ly6C^+ subtype, and the F4/80^+
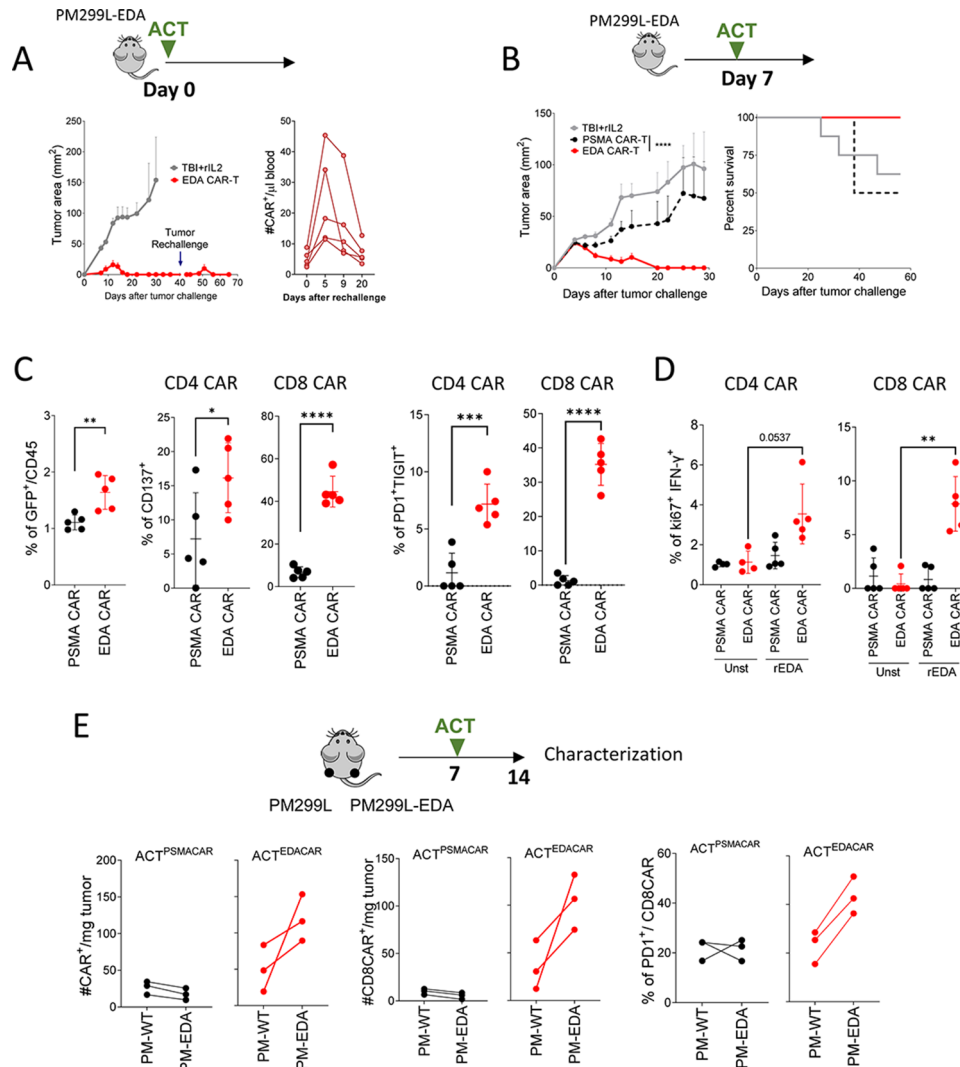
Figure 4 Antitumor activity of EDA CAR-T therapy in EDA⁺ tumors. (A) C57BL/6 J mice were injected subcutaneously with 2×10⁶ cells PM299L-EDA^high tumor cells. Four hours later, mice were treated with EDA CAR-T. At day 40, mice were rechallenged with PM299L-EDA^high tumor cells. mean tumor are is ploted (left panel). EDA CAR-T cell expansion measured in blood of mice after tumor rechallenge (right panel). (B) C57BL/6 J mice were injected subcutaneously with 2×10⁶ cells PM299L-EDA^high tumor cells. At day 7, mice-bearing tumors were treated by adoptive transfer with 9×10⁶ EDA CAR-T or with PSMA CAR-T cells as a control. Tumor growth and Kaplan-Meier survival curves are represented (n=7 mice per group). Data are representative of two independently repeated experiments. (C) Percentage of tumor infiltrating CAR-T cells and expression of CD137, PD1 and TIGIT in PSMA CAR-T and EDA CAR-T cells. (D) Percentage of proliferating (Ki67⁺ IFN-γ⁺) CD4⁺ and CD8⁺ EDA CAR-T and PSMA CAR-T cells isolated from the spleen of mice-bearing tumors in response to EDA stimulation. (n=4 mice per group). (E) Migratory capacity of the infused CAR-T to the site of antigen expression. Mice-bearing the PM299L-EDA^high in the right flank and the original PM299L tumor cell line (EDA negative) in the left flank were treated intravenously with EDA CAR-T or PSMA CAR-T cells and 7 days later, the CAR-T cells infiltrating each tumor were analyzed by flow cytometry. Data are representative of two independently repeated experiments. *P<0,05, **p<0.01, ***p<0005, ****p<0001. Survival curve were analyzed by logrank test (A, B). Student's t-test (C). One-way ANOVA with the Bonferroni multiple comparisons test (D). Bars representing the mean and SD are plotted. Each symbol represents an individual mouse. CAR-T, chimeric antigen receptor T-cell; EDA, extra domain A.

cells, in particular the CD206⁺ (M2 subtype) in mice treated with EDA CAR-T cells. No significant changes were observed regarding the number of intratumor Treg cells or the endogenous CD4 or CD8 T cells (online supplemental figure 6). The antitumor effect of EDA CAR-T cell administration was not observed in C57BL/6 mice-bearing B16OVA tumors (negative for EDA) (online supplemental figure 7).

To more deeply understand this antitumor activity, we studied the effect of EDA CAR-T therapy in the tumor microenvironment. Since EDA is expressed close to the tumor endothelium in this model (online supplemental figure 3C), we evaluated the effect of EDA CAR-T on the tumor vasculature by using AngioSense, a fluorescent probe designed to evaluate tumor vascular changes and blood vessel density in vivo. Tumor vasculature was
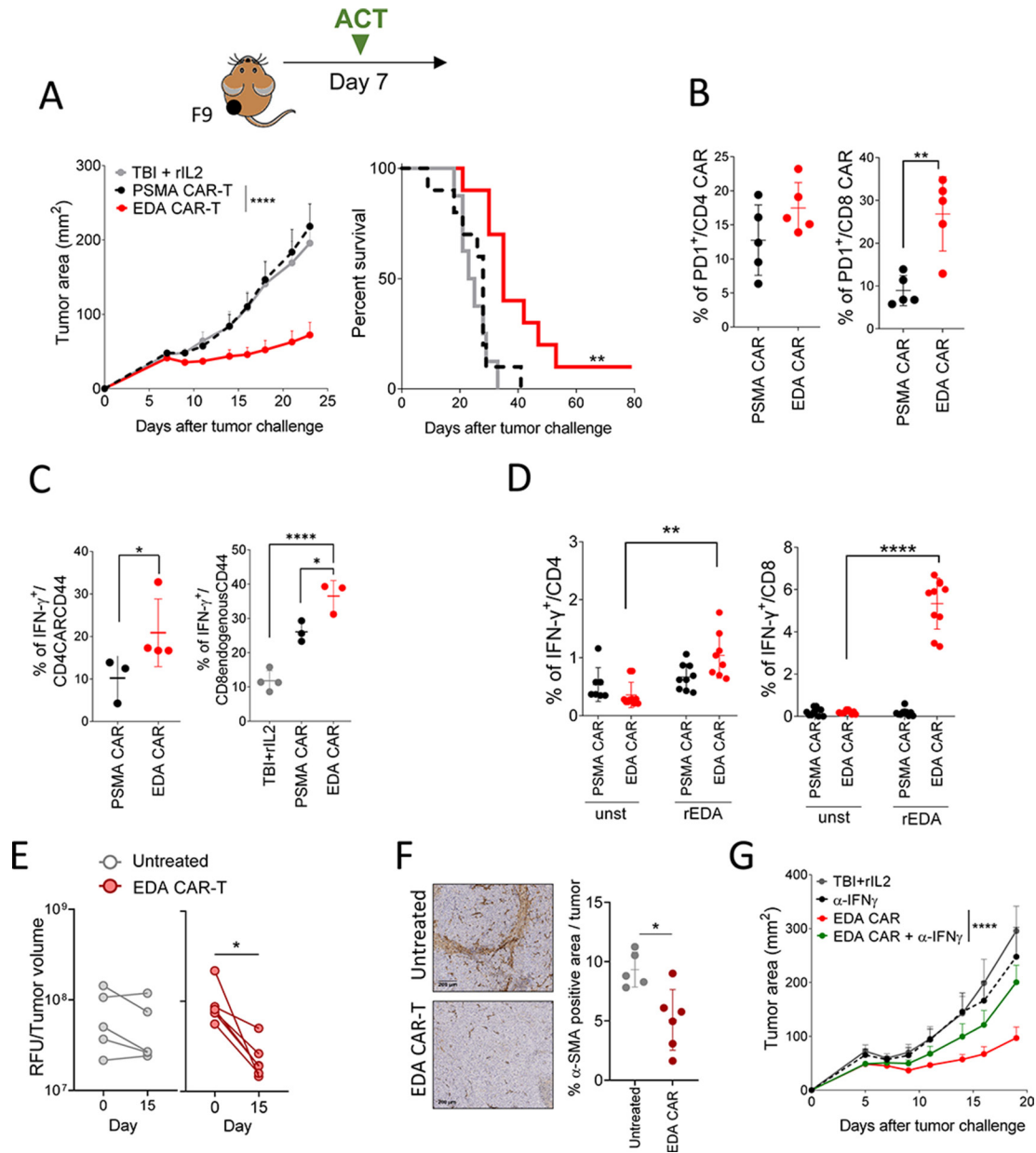
Figure 5 EDA CAR-T cells delay F9 teratocarcinoma tumor growth. (A) 129SV mice-bearing F9 tumor cells (n=10 mice per group) were treated with a single dose of 1×10^7 of EDA CAR-T or PSMA CAR-T cells. tumor growth at different time points (left) and Kaplan-Meier plot of survival of mice-bearing tumors (right) are plotted. (B) Characterization of PD1+ CAR-T cells infiltrating the tumor 7 days after cell transfer (n=5). (C) Percentage of IFN-γ producing CD4 CAR-T or CD8 endogenouse cells in the draining lymph nodes after a short stimulation with PMA/ionomycin. (D) Percentage of IFN-γ in CD4 and CD8 after short stimulation with recombinant EDA protein coated plate. (E) Direct in vivo estimation of tumor vasculature using Angiosense 750 at days −1 and 14 after EDA CAR-T-cell infusion, expressed as relative fluorescence units divided by tumor volume in 129SV mice-bearing F9 subcutaneous tumors. untreated mice were used as negative control (n=5–6 mice/group). (F) α-SMA immunohistochemistry analysis on tumor samples at day 14 after EDA CAR-T therapy. Two representative images for untreated and EDA CAR-T treated mice and the quantification of α-SMA positive area are shown. Data are representative of two independent experiments. (G) Effect of IFN-γ neutralization on the antitumor effect of EDA CAR-T cell infusion. *P<0,05, **p<0.01, ****p<0.0001. (A) Survival curve was analyzed by the log-rank test. Student's t-test (B, C, F) One-way ANOVA with Bonferroni multiple comparisons test (C, D). Paired t-test (E). Nonlinear regression analysis (G). The mean and SD for each group are plotted. Each symbol represents an individual mouse. CAR-T, chimeric antigen receptor T-cell; EDA, extra domain A.

measured in mice-bearing F9 tumors before and 14 days after the adoptive transfer of EDA CAR-T cells. Quantitative relative fluorescence units divided by tumor volume were analyzed for each animal at these two time points. Importantly, it was found that while no significant changes were observed in the intratumor fluorescence accumulation in untreated mice, a significant reduction in fluorescence was found in those mice treated with EDA CAR-T cells, indicating an antiangiogenic activity for this CAR-T (figure 5E). We also found a significant reduction
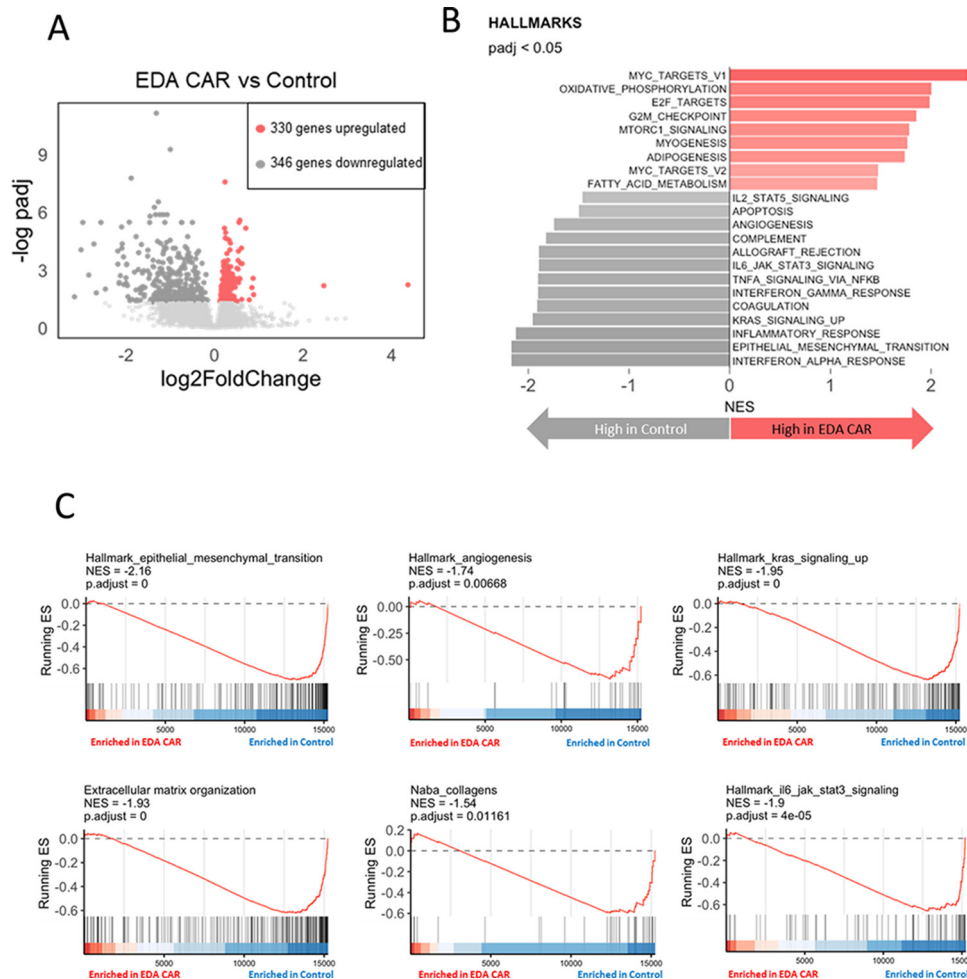
Figure 6 Transcriptomic analysis of tumor tissues isolated from untreated mice and from mice treated with EDA CAR-T cells. 129SV mice-bearing F9 tumor cells were treated with EDA CAR-T or left untreated and 14 days after adoptive cell transfer, mRNA from tumor samples was isolated for RNASec analysis. (A) Volcano plots for differential gene expression of control vs EDA CAR-T cell treated mice. Genes with a padj <0.05 were considered differentially expressed. (B) Hallmark gene set enrichment analysis with positive and negative enrichment scores for specific biological states in untreated and EDA CAR-T treated mice. (C) Selected gene sets with a significant negative enrichment in tumors treated with EDA CAR-T cells. FDR Q values were calculated using GSEA software. CAR-T, chimeric antigen receptor T-cell; EDA, extra domain A. FDR, Fale Discovery Rate.

on α-SMA staining in tumor samples of mice treated with EDA CAR-T cells, supporting the potential impact of EDA targeting on myofibroblast differentiation and tumor stromal density (figure 5F). Since IFN-γ is one of the major antifibrotic factors[24] and display antiangiogenic activity,[25] we carried out a new in vivo assay to evaluate the antitumor activity of EDA CAR-T when mice were also treated with neutralizing anti-IFN-γ antibodies (i.p. injection of 100 µg/mouse at days 1, 4, 8 and 12 after EDA CAR-T transfer). This treatment, significantly abrogated the antitumor activity of EDA CAR-T adoptive transfer (figure 5G).

To better characterize the tumor microenvironment after adoptive cell therapy, we carried out a transcriptomic analysis of tumor tissues isolated from untreated and EDA CAR-T treated mice (14 days after adoptive transfer). We found 330 genes upregulated and 346 genes downregulated in tumors treated with EDA CAR-T as compared

with untreated tumors (figure 6A). In agreement with the results obtained in the immunohistochemical analyses, GSEA enrichment analysis when compared EDA CAR-T treated versus untreated mice showed a significant negative enrichment in gene sets defining epithelial-mesenchymal transition (systematic name: M5930), genes encoding collagen proteins (M3005) or genes upregulated during formation of blood vessels (angiogenesis; M5944). We also found a significant negative enrichment in gene sets defining inflammatory processes, including Il2-STAT5, IL6-JAK-STAT3. TNF-α, IFN-γ, IFN-α or KRAS signaling, suggesting a great impact on the tumor inflammatory profile after EDA CAR-T transfer (figure 6B,C).

Safety of EDA CAR-T cells
To assess the safety of EDA CAR-T, healthy mice were injected with 1×10^7 EDA CAR-T cells. EDA CAR-T cell transfer in these mice did not result in apparent toxicity

for the mice. We detected no weight loss during 30 days of follow-up after ACT. No significant changes between groups were found for AST, ALT, serum albumin, AMYL2, urea, creatinine, CRPLX, ALP or LDH levels at days 17 and 30 after T cell infusion (online supplemental figure 8A) and no histological differences were observed between tissues examined from both groups at day 30 (online supplemental figure 8B). We also evaluated the potential expansion of EDA CAR-T cells in non-tumor-bearing mice that received a single intravenous dose of 1×10^7 EDA CAR-T cells or PSMA CAR-T expressing Luciferase as a reporter gene. In vivo bioluminescence was visualized using the PhotonImager Optima at days 1, 3, 7, 10 and 14 after T cell infusion. No specific expansion of EDA CAR-T lymphocytes was observed in mice at any of the times studied, suggesting that EDA CAR-T cells do not detect EDA antigen in a healthy mouse (online supplemental figure 8C). Then, we studied the EDA expression in two pathogenic conditions such as an animal model of liver fibrosis and a model of inflammatory colitis. Liver samples from mice with fibrosis induced by CCL4 treatment, or colon samples from mice with DSS-induced colitis were stained with F8 anti-EDA scFv. The corresponding tissue sections from untreated healthy mice were used as controls. EDA expression was not detected in these pathological conditions (online supplemental figure 8D).

We also analyzed the expression of EDA in human liver samples with different types of liver cirrhosis. We included three samples from patients with alcoholic cirrhosis, two patients with Hepatitis C virus (HCV) and two Hepatitis B Virus (HBV)-related cirrhosis, four primary biliary cirrhosis, two autoimmune and one cryptogenic cirrhosis. As control, we included one healthy liver sample and two patients with HCC. It was found that none of these conditions showed a remarkable expression of EDA, compared with the EDA expression observed in hepatocarcinoma (online supplemental figure 8E), indicating that EDA expression is very restricted in adult tissues and suggesting that EDA CAR-T cell therapy could be safe.

EDA CAR-T cells exerts antitumor activity in a xenograft mouse model of human hepatocarcinoma

We generated a lentiviral construct encoding the EDA CAR consisting of the anti-EDA F8 scFv, a short hinge/CD28 transmembrane domain, and the human 41BB and the CD3ζ endodomains. An anti-human BCMA CAR was prepared using the same backbone and used as an irrelevant CAR construct. Human EDA CAR and BCMA CAR-T cells generated by lentiviral transduction of T cells purified from healthy donors express the EDA CAR on their surface and bind human EDA-His protein (figure 7A). The triple parameter T cell reporter Jurkat cell line transduced with the LV expressing human EDA CAR activated NFAT, AP1 and NF-kB transcription factors when they were stimulated with EDA-coated plates (figure 7B). In agreement with these data, we also observed that EDA CAR-T cells produced TNF-α, IFN-γ and IL-2 and

proliferated in response to increasing amounts of EDA (figure 7C).

The human hepatocarcinoma cell line PLC xenografted in NSG mice expressed high levels of EDA in the tumor stroma and in the CD31-expressing endothelial cells (figure 1F). To evaluate if the human EDA CAR-T cells could exert an antitumoral effect in this tumor model, NSG mice xenografted with PLC cell line were treated with 5×10^6 CAR-T cells, with 5×10^6 untransduced T cells or left untreated. The main problem with the use of NSG mice injected with human PBMC is the rapid development of graft-versus-host disease, whose kinetics limit the duration of the study and the interpretation of the results.[26] Indeed, the median survival time of NSG mice after intravenous injection of fresh human PBMC is 30–40 days.[26 27] Despite this limitation, xenograft models are instrumental to establish the first proof of concept for CAR-T cell therapies. Importantly, mice treated with EDA CAR were able to stop tumor growth until the end of the experiment at day 35 (figure 7D). In a parallel experiment, we characterized the phenotype of the EDA CAR-T cells 8 days after the T cell infusion. CAR-T cells present in the spleen and into the tumor were analyzed by flow cytometry for the expression of activation (CD137, GzmB and ICOS) and exhaustion (PD1, TIGIT and Lag3) markers. There was a significant increase in the percentage of cells expressing one, two or three activation markers in CAR-T cell isolated from the tumor with respect to those isolated from the spleen, suggesting that the antigen encountered into the tumor activated the CAR-T cells. Notably, these tumor infiltrating EDA CAR-T cells also expressed exhaustion markers (figure 7E).

DISCUSSION

One of the main challenges for the translation of CAR-T cell-based therapies for solid tumors is the identification of specific antigens expressed in the tumor cell membrane. In this effort, it is necessary to explore other alternative antigens present in the tumor microenvironment, even if they are not expressed by the tumor cell itself. One promising target is fibronectin and its spliced versions, which are key in the reorganization of the tumor ECM to promote tumor growth, migration, invasion and to impair tumor cell responsiveness to therapy.[8] In this study, we focused on the oncofetal form of FN containing EDA, which has been shown to be expressed in many tumor types while it is undetectable in normal tissues.[10] From the TCGA SpliceSeq analysis as well as from the RNAseq analysis of HCC samples, we have confirmed the upregulation of the EDA in several tumor types. Our immunohistochemical analysis in biopsies from different tumor types, confirmed the positive staining for EDA in tumor stroma and vessels from cholangiocarcinoma, hepatocarcinoma, colon, ovarian or in pancreatic carcinoma, expanding the previous results on the strong EDA staining of vascular structures in a panel of human
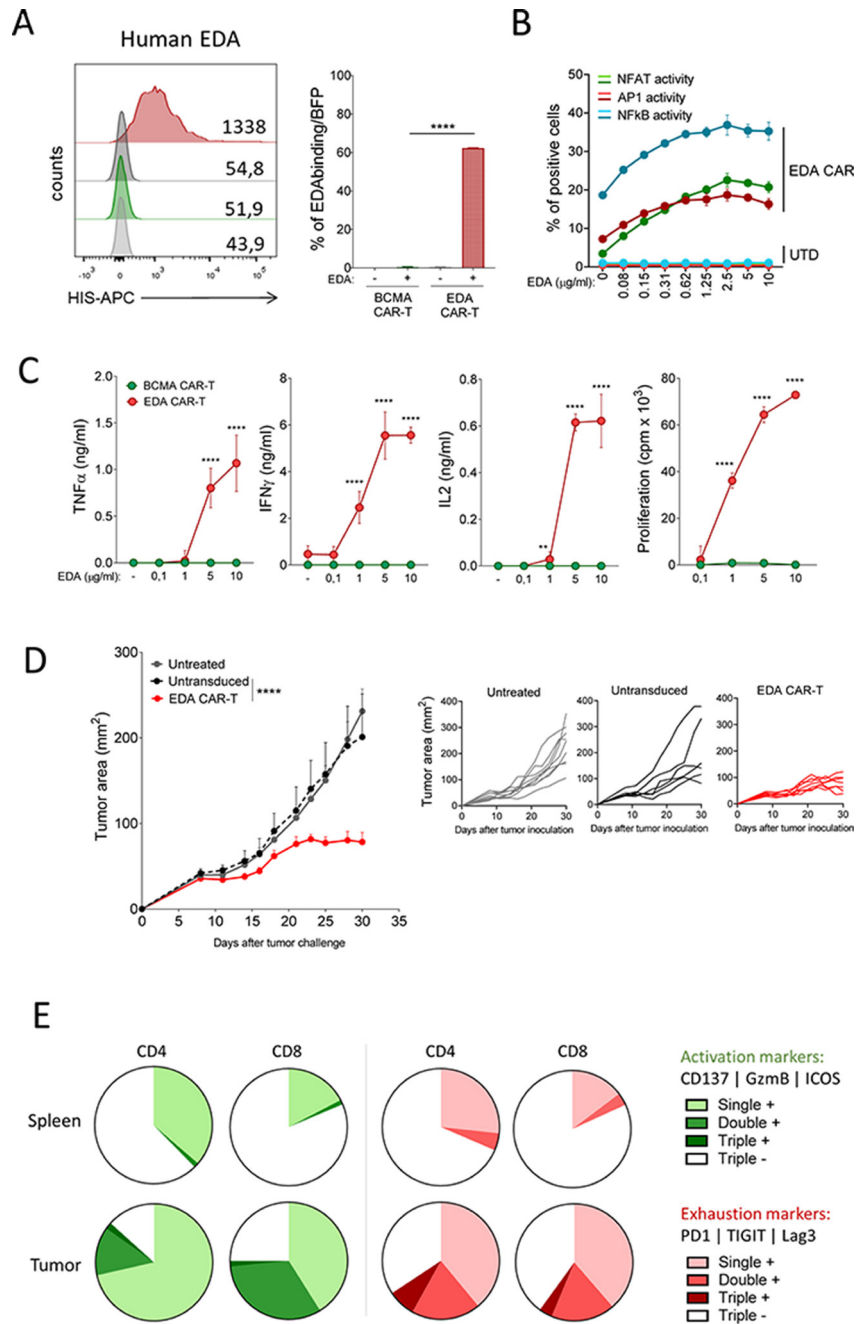
Figure 7 EDA CAR-T cells have antitumor activity in NSG mice xenotransplanted with the human hepatocarinoma cell line PLC. (A) Human EDA CAR binding to EDA protein measured by flow cytometry. numbers in histogram indicate mean fluorescence intensity. (B) Flow cytometric analysis of the activation of NFAT, AP1 and NF-kB in the triple parameter T cell reporter Jurkat cell line expressing the human EDA CAR in response to different doses of the EDA protein. (C) Cytokine production and proliferation of human EDA CAR-T or a control CAR-T cells in response to EDA stimulation. (D) Antitumor activity in NSG mice xenotransplanted with the human hepatocarinoma cell line PLC. NSG mice (n=6–9 mice per group) were challenged with PLC tumor cells and, 8 days later, when the tumors reached 5 mm in diameter, mice were treated with 5×10^6 untransduced or EDA CAR transduced T cells. (D) Mean tumor area at different time points (left) and tumor area of each individual mouse in each experimental group (right). (E) phenotypic analysis of CD4 or CD8 EDA CAR-T cells isolated from the spleen or tumors, 7 days after adoptive transfer. activation markers (in green) and exhaustion markers (in red) were analyzed by flow cytometry. data are representative of two independently repeated experiments. ****$P<0.0001$. Two-way ANOVA with the Bonferroni multiple comparisons test. The mean and SD for each condition are plotted. CAR-T, chimeric antigen receptor T-cell; EDA, extra domain A.

tumors[16][28] and supporting the potential use of EDA as a tumor target antigen.

The aberrant vasculature[29][30] and the fibrotic state of desmoplastic tumors can impair lymphocyte tumor infiltration. It is accepted that carcinomas behave like wounds, which force the TME into a constant state of fibrotic repair[31] with a continuous and extensive remodeling of ECM. This highly fibrotic structure, with the accumulation of extensively crosslinked type I collagen fibrils,[32] significantly affects tumor progression, metastasis and response-to-therapy[5][33][34] being a biomarker of poor outcome.[35] This collagen fibrillogenesis is supported by fibronectin networks that may provide a template for deposition of collagen and other components of the ECM. Notably, FN in perivascular matrices constitutes an obligate scaffold for organization of the vessel-associated ECM and a repository for proangiogenic factors.[36] The excessive deposition of collagen and FN around tumor islets significantly impair T cell motility and tumor infiltration[6][37] by acting as a shield between T cells and tumor cells. EDA-containing FN plays a relevant role in collagen deposition and α-SMA expression by myofibroblasts, probably by its direct implication in latent TGF-β activation.[38] The presence of EDA highly correlated with enhanced matrix remodeling and reorganization of the actin cytoskeleton,[39] pointing toward a profibrotic role for EDA in the tumor ECM. For these reasons, we consider EDA as a relevant target for CAR-T therapies, especially in the so-called 'cold' or 'immune excluded' tumors,[40] where antitumor lymphocytes do not access the tumor bed probably because of the mechanical barrier function of the ECM and the aberrant tumor vasculature. In fact, it has been demonstrated that FN-EDA plays an important role in the development of pathological neoangiogenesis[41][42] promoting intratumoral microvessel formation and tumor progression.[43]

We have demonstrated that EDA CAR-T cells can recognize EDA-expressing tumor cells and prevent tumor growth in vivo. But notably, EDA CAR-T cell infusion showed antitumor therapeutic efficacy against the challenge with tumor cells not expressing EDA. The CD31/EDA colocalization experiments suggest a localization of EDA in the tumor ECM and in the basement membrane surrounding and supporting the tumor endothelial cells. The antitumor activity of EDA CAR-T seems to be mediated by IFN-γ. This cytokine might have a direct effect on tumor cells by (1) inhibiting cell proliferation or sensitizing cells to apoptosis,[44][45] (2) upregulating MHC class I expression and thereby increasing tumor cell lysis by endogenous antitumor T cells[46]; (3) stimulating NK activity,[47] or (4) inhibiting angiogenesis.[25][48] We did not found any inhibitory effect of IFN-γ on proliferation of F9 tumor cells in vitro even at doses of 5000 U/mL (not shown). Upregulation of MHC class I molecules, the susceptibility to CTL-dependent lysis or the activation of NK cells may not be the main mechanisms since we did not found a significant increase of endogenous T cells after EDA CAR-T therapy. Moreover, EDA CAR-T cells also showed an antitumor effect in NSG mice challenged with human PLC tumor cell line. Thus, it can be speculated that the IFN-γ-dependent antiangiogenic activity may constitute an important mechanism of action of the EDA CAR-T cells.

RNAseq analysis revealed an important effect of EDA CAR-T therapy in the tumor microenvironment with a significant reduction in gene signatures associated with epithelial-mesenchymal transition, genes encoding collagen proteins or genes upregulated during formation of blood vessels as well as in gene sets defining inflammatory processes. Chronic inflammation generated by the tumor microenvironment is known to drive cancer initiation, proliferation, progression, metastasis, and therapeutic resistance.[49] Notably, we found that EDA CAR-T promoted a significant reduction in the IL-6-STAT5 and the KRAS related signatures that has been associated to a poor prognosis in many cancers.[50][51] The important reduction in the expression of gene sets associated with inflammation might be in agreement with the observed increase in the number of M2 macrophages (M2 TAMs) infiltrating the tumor after EDA CAR-T cell therapy. Although most of the published works point to M2 TAM as an anti-inflammatory and protumor element associated with a poor prognosis, we do not know if this observed increase in M2 TAM is playing a role in the antitumor action of EDA CAR-T or if it is a consequence of the changes that the therapy is producing in TME. It has been described that an increase in TAMs exhibiting an M2-phenotype can contribute to resistance to anti-angiogenic therapies,[52] chemotherapies,[53] radiotherapies[54] or immunotherapies.[55] Given the importance of M2 TAM in regulating tumor immunity, there has been considerable interest in therapeutic strategies that target macrophages, either by their depletion or by altering their protumoral activities. However, since this classification into the antitumor M1 and the protumor M2 TAMs, transcriptional, epigenetic and metabolomic studies have revealed the complexity of macrophage differentiation with important overlapping in gene expression, highlighting a continuum rather than definite proinflammatory and anti-inflammatory functional states.[56] Further experiments will be needed to understand if TAM depletion could favor the antitumor activity of the EDA CAR-T cell therapies.

There is also evidence for an immunosuppressive function of EDA through the recruitment of Treg cells[57] or the activation of myeloid-derived suppressor cells,[58] that weaken the immune response against cancer confirming its protumor effect. All these functions induced by FN-EDA might be elicited through its binding to the integrins α4β1, α4β7,[59] α9β1,[60] α5β1[61] or to TLR4[62] displaying a direct protumorigenic activity.[63][64] Other CAR-T cells attempt to disrupt tumor neovasculature by targeting α5β3 integrin,[65] TEM8[66][67] or CLEC14A,[68] although some toxicity issues have been also arisen[67][69] probably because of the 'on-target off-tumor' activity of the CAR-T.

It is plausible that EDA secretion by tumor cells or tumor infiltrating cells enabled EDA CAR-T cells to target tumor

vasculature that express the potential EDA receptors such as some integrins or TLR4. We tested this possibility using the Jurkat TPR system, which allows to evaluate T cell activation primed by EDA CAR after antigen recognition. First, we confirmed that EDA proteins binds to the cell surface of wild type Jurkat cells, which express high levels of integrins α4β1 among others.[70] We then tested if these wild type Jurkat cells previously incubated with soluble EDA protein could activate the NFAT, AP1 or NF-kB signaling in the TPR Jurkat cells transduced with EDA CAR. Using this reporter assay we found a significant activation of NFAT, AP1 and KF-kB in TPR reporter cells in the presence of EDA-coated Jurkat cells, supporting a potential indirect recognition of cells able to bind EDA produced within the tumor (online supplemental figure 9). A similar strategy has recently been proposed using CAR-T cells against the EDB of fibronectin, showing also antitumor and antivascular activity in preclinical mouse tumor models.[71 72] Both extra domains have been shown to be highly expressed in several tumors and tumor neovasculature, suggesting a role in tumor progression. However, it is becoming clear that the alternatively spliced EDA and EDB domains may exert different functions.[10]

We did not observe any clinical signs of toxicity in the EDA CAR-T cell treated animals suggesting that EDA is not expressed in healthy tissues, at least at the level needed for CAR-T cell activation, and also that EDA CAR-T cells are well-tolerated with no noticeable 'on-target/off-tumor' toxicity. Human EDA CAR-T cells exerted a strong antitumoral effect in an NSG xenograft model for human hepatocarcinoma, suggesting a potential translation to human settings for the treatment of human tumors with upregulated EDA expression.

Author affiliations
[1] Programa de Inmunología e Inmunoterapia, Centro de Investigación Médica Aplicada, Pamplona, Spain
[2] Programa de Tumores sólidos, Centro de Investigación Médica Aplicada, Pamplona, Spain
[3] Instituto de Investigación Sanitaria de Navarra, Pamplona, Spain
[4] Departamento de Patología, Clinica Universidad de Navarra, Pamplona, Navarra, Spain
[5] Programa de Hemato-Oncología, Centro de Investigación Médica Aplicada, CIMA, Pamplona, Spain
[6] Centro de Investigacion Biomedica en Red de Cancer (CIBERONC), Madrid, Spain
[7] Departamento de Hematología, Clínica Universidad de Navarra, Pamplona, Spain
[8] Cancer Center Universidad de Navarra (CCUN), Universidad de Navarra, Pamplona, Spain

ORCID iDs
Alfonso Calvo http://orcid.org/0000-0003-4074-4242
Sandra Hervas-Stubbs http://orcid.org/0000-0003-3391-1516
Juan Jose Lasarte http://orcid.org/0000-0003-1641-3881

REFERENCES
1. Brentjens RJ, Davila ML, Riviere I, et al. CD19-targeted T cells rapidly induce molecular remissions in adults with chemotherapy-refractory acute lymphoblastic leukemia. *Sci Transl Med* 2013;5:177ra38.
2. Grupp SA, Kalos M, Barrett D, et al. Chimeric antigen receptor-modified T cells for acute lymphoid leukemia. *N Engl J Med* 2013;368:1509–18.
3. Wagner J, Wickman E, DeRenzo C, et al. Car T cell therapy for solid tumors: bright future or dark reality? *Mol Ther* 2020;28:2320–39.
4. Caruana I, Savoldo B, Hoyos V, et al. Heparanase promotes tumor infiltration and antitumor activity of CAR-redirected T lymphocytes. *Nat Med* 2015;21:524–9.
5. Jiang H, Hegde S, DeNardo DG. Tumor-Associated fibrosis as a regulator of tumor immunity and response to immunotherapy. *Cancer Immunol Immunother* 2017;66:1037–48.
6. Salmon H, Franciszkiewicz K, Damotte D, et al. Matrix architecture defines the preferential localization and migration of T cells into the stroma of human lung tumors. *J Clin Invest* 2012;122:899–910.
7. Tahkola K, Ahtiainen M, Mecklin J-P, et al. Stromal hyaluronan accumulation is associated with low immune response and poor prognosis in pancreatic cancer. *Sci Rep* 2021;11:12216.
8. Efthymiou G, Saint A, Ruff M, et al. Shaping up the tumor microenvironment with cellular fibronectin. *Front Oncol* 2020;10:641.
9. Wang JP, Hielscher A. Fibronectin: how its aberrant expression in tumors may improve therapeutic targeting. *J Cancer* 2017;8:674–82.

10 Kumra H, Reinhardt DP. Fibronectin-targeted drug delivery in cancer. *Adv Drug Deliv Rev* 2016;97:101–10.

11 Moschetta M, Pretto F, Berndt A, *et al*. Paclitaxel enhances therapeutic efficacy of the F8-IL2 immunocytokine to EDA-fibronectin-positive metastatic human melanoma xenografts. *Cancer Res* 2012;72:1814–24.

12 Rosini E, Volpi NA, Ziffels B, *et al*. An antibody-based enzymatic therapy for cancer treatment: the selective localization of D-amino acid oxidase to EDA fibronectin. *Nanomedicine* 2021;36:102424.

13 Ryan MC, Cleland J, Kim R, *et al*. SpliceSeq: a resource for analysis and visualization of RNA-Seq data on alternative splicing and its functional impacts. *Bioinformatics* 2012;28:2385–7.

14 Ryan M, Wong WC, Brown R, *et al*. TCGASpliceSeq a compendium of alternative mRNA splicing in cancer. *Nucleic Acids Res* 2016;44:D1018–22.

15 Jutz S, Leitner J, Schmetterer K, *et al*. Assessment of costimulation and coinhibition in a triple parameter T cell reporter line: simultaneous measurement of NF-κB, NFAT and AP-1. *J Immunol Methods* 2016;430:10–20.

16 Rybak J-N, Roesli C, Kaspar M, *et al*. The extra-domain a of fibronectin is a vascular marker of solid tumors and metastases. *Cancer Res* 2007;67:10948–57.

17 Lasarte JJ, Casares N, Gorraiz M, *et al*. The extra domain A from fibronectin targets antigens to TLR4-expressing cells and induces cytotoxic T cell responses in vivo. *J Immunol* 2007;178:748–56.

18 Casares N, Rudilla F, Arribillaga L, *et al*. A peptide inhibitor of FOXP3 impairs regulatory T cell activity and improves vaccine efficacy in mice. *J Immunol* 2010;185:5150–9.

19 Lozano T, Chocarro S, Martin C, *et al*. Genetic Modification of CD8⁺ T Cells to Express EGFR: Potential Application for Adoptive T Cell Therapies. *Front Immunol* 2019;10:2990.

20 Madri JA. Extracellular matrix modulation of vascular cell behaviour. *Transpl Immunol* 1997;5:179–83.

21 Balza E, Borsi L, Allemanni G, *et al*. Transforming growth factor beta regulates the levels of different fibronectin isoforms in normal human cultured fibroblasts. *FEBS Lett* 1988;228:42–4.

22 Ventura E, Weller M, Macnair W, *et al*. TGF-β induces oncofetal fibronectin that, in turn, modulates TGF-β superfamily signaling in endothelial cells. *J Cell Sci* 2018;131:jcs209619.

23 Winn HJ. Immune mechanisms in homotransplantation. II. quantitative assay of the immunologic activity of lymphoid cells stimulated by tumor homografts. *J Immunol* 1961;86:228–39.

24 van Dijk F, Olinga P, Poelstra K, *et al*. Targeted therapies in liver fibrosis: combining the best parts of platelet-derived growth factor BB and interferon gamma. *Front Med* 2015;2:72.

25 Coughlin CM, Salhany KE, Gee MS, *et al*. Tumor cell responses to IFNgamma affect tumorigenicity and response to IL-12 therapy and antiangiogenesis. *Immunity* 1998;9:25–34.

26 Ali N, Flutter B, Sanchez Rodriguez R, *et al*. Xenogeneic graft-versus-host-disease in NOD-scid IL-2Rγnull mice display a T-effector memory phenotype. *PLoS One* 2012;7:e44219.

27 Courtois J, Ritacco C, Dubois S, *et al*. Itacitinib prevents xenogeneic GVHD in humanized mice. *Bone Marrow Transplant* 2021;56:2672–81.

28 Glukhova MA, Frid MG, Shekhonin BV, *et al*. Expression of fibronectin variants in vascular and visceral smooth muscle cells in development. *Dev Biol* 1990;141:193–202.

29 Bergers G, Benjamin LE. Tumorigenesis and the angiogenic switch. *Nat Rev Cancer* 2003;3:401–10.

30 Itatani Y, Kawada K, Yamamoto T, *et al*. Resistance to anti-angiogenic therapy in Cancer-Alterations to anti-VEGF pathway. *Int J Mol Sci* 2018;19:1232.

31 Dvorak HF. Tumors: wounds that do not heal. similarities between tumor stroma generation and wound healing. *N Engl J Med* 1986;315:1650–9.

32 Perryman L, Erler JT. Lysyl oxidase in cancer research. *Future Oncol* 2014;10:1709–17.

33 Keely PJ. Mechanisms by which the extracellular matrix and integrin signaling act to regulate the switch between tumor suppression and tumor promotion. *J Mammary Gland Biol Neoplasia* 2011;16:205–19.

34 Werb Z, Lu P. The role of stroma in tumor development. *Cancer J* 2015;21:250–3.

35 Paszek MJ, Zahir N, Johnson KR, *et al*. Tensional homeostasis and the malignant phenotype. *Cancer Cell* 2005;8:241–54.

36 Van Obberghen-Schilling E, Tucker RP, Saupe F, *et al*. Fibronectin and tenascin-C: accomplices in vascular morphogenesis during development and tumor growth. *Int J Dev Biol* 2011;55:511–25.

37 Joyce JA, Fearon DT. T cell exclusion, immune privilege, and the tumor microenvironment. *Science* 2015;348:74–80.

38 Muro AF, Moretti FA, Moore BB, *et al*. An essential role for fibronectin extra type III domain A in pulmonary fibrosis. *Am J Respir Crit Care Med* 2008;177:638–45.

39 Saito S, Yamaji N, Yasunaga K, *et al*. The fibronectin extra domain a activates matrix metalloproteinase gene expression by an interleukin-1-dependent mechanism. *J Biol Chem* 1999;274:30756–63.

40 Salerno EP, Bedognetti D, Mauldin IS, *et al*. Human melanomas and ovarian cancers overexpressing mechanical barrier molecule genes lack immune signatures and have increased patient mortality risk. *Oncoimmunology* 2016;5:e1240857.

41 Su X, Ma X, Xie X, *et al*. FN-EDA mediates angiogenesis of hepatic fibrosis via integrin-VEGFR2 in a CD63 synergetic manner. *Cell Death Discov* 2020;6:140.

42 Xiang L, Xie G, Ou J, *et al*. The extra domain A of fibronectin increases VEGF-C expression in colorectal carcinoma involving the PI3K/Akt signaling pathway. *PLoS One* 2012;7:e35378.

43 Lv W-Q, Wang H-C, Peng J, *et al*. Gene editing of the extra domain a positive fibronectin in various tumors, amplified the effects of CRISPR/Cas system on the inhibition of tumor progression. *Oncotarget* 2017;8:105020–36.

44 Langaas V, Shahzidi S, Johnsen JI, *et al*. Interferon-Gamma modulates TRAIL-mediated apoptosis in human colon carcinoma cells. *Anticancer Res* 2001;21:3733–8.

45 Mazzolini G, Narvaiza I, Martinez-Cruz LA, *et al*. Pancreatic cancer escape variants that evade immunogene therapy through loss of sensitivity to IFNgamma-induced apoptosis. *Gene Ther* 2003;10:1067–78.

46 Dighe AS, Richards E, Old LJ, *et al*. Enhanced in vivo growth and resistance to rejection of tumor cells expressing dominant negative IFN gamma receptors. *Immunity* 1994;1:447–56.

47 Brunda MJ, Rosenbaum D. Modulation of murine natural killer cell activity in vitro and in vivo by recombinant human interferons. *Cancer Res* 1984;44:597–601.

48 Qin Z, Schwartzkopff J, Pradera F, *et al*. A critical requirement of interferon gamma-mediated angiostasis for tumor rejection by CD8+ T cells. *Cancer Res* 2003;63:4095–100.

49 Quinn KM, Kartikasari AER, Cooke RE, *et al*. Impact of age-, cancer-, and treatment-driven inflammation on T cell function and immunotherapy. *J Leukoc Biol* 2020;108:953–65.

50 Caetano MS, Zhang H, Cumpian AM, *et al*. Il6 blockade reprograms the lung tumor microenvironment to limit the development and progression of K-ras-Mutant lung cancer. *Cancer Res* 2016;76:3189–99.

51 Johnson DE, O'Keefe RA, Grandis JR. Targeting the IL-6/JAK/STAT3 signalling axis in cancer. *Nat Rev Clin Oncol* 2018;15:234–48.

52 Castro BA, Flanigan P, Jahangiri A, *et al*. Macrophage migration inhibitory factor downregulation: a novel mechanism of resistance to anti-angiogenic therapy. *Oncogene* 2017;36:3749–59.

53 Dijkgraaf EM, Heusinkveld M, Tummers B, *et al*. Chemotherapy alters monocyte differentiation to favor generation of cancer-supporting M2 macrophages in the tumor microenvironment. *Cancer Res* 2013;73:2480–92.

54 Choi S-H, Kim A-R, Nam J-K, *et al*. Tumour-vasculature development via endothelial-to-mesenchymal transition after radiotherapy controls CD44v6⁺ cancer cell and macrophage polarization. *Nat Commun* 2018;9:5108.

55 Zhang M, Huang L, Ding G, *et al*. Interferon gamma inhibits CXCL8-CXCR2 axis mediated tumor-associated macrophages tumor trafficking and enhances anti-PD1 efficacy in pancreatic cancer. *J Immunother Cancer* 2020;8:e000308.

56 Goswami S, Anandhan S, Raychaudhuri D, *et al*. Myeloid cell-targeted therapies for solid tumours. *Nat Rev Immunol* 2022. doi:10.1038/s41577-022-00737-w. [Epub ahead of print: 13 Jun 2022].

57 Sengupta S, Nandi S, Hindi ES, *et al*. Short hairpin RNA-mediated fibronectin knockdown delays tumor growth in a mouse glioma model. *Neoplasia* 2010;12:837–47.

58 Rossnagl S, Altrock E, Sens C, *et al*. EDA-Fibronectin originating from osteoblasts inhibits the immune response against cancer. *PLoS Biol* 2016;14:e1002562.

59 Liao Y-F, Gotwals PJ, Koteliansky VE, *et al*. The EIIIA segment of fibronectin is a ligand for integrins alpha 9beta 1 and alpha 4beta 1 providing a novel mechanism for regulating cell adhesion by alternative splicing. *J Biol Chem* 2002;277:14467–74.

60 Sun X, Fa P, Cui Z, *et al*. The EDA-containing cellular fibronectin induces epithelial-mesenchymal transition in lung cancer cells through integrin α9β1-mediated activation of PI3-K/Akt and ERK1/2. *Carcinogenesis* 2014;35:184–91.

61 Manabe R, Ohe N, Maeda T, *et al*. Modulation of cell-adhesive activity of fibronectin by the alternatively spliced EDA segment. *J Cell Biol* 1997;139:295–307.

62 Okamura Y, Watari M, Jerud ES, *et al*. The extra domain A of fibronectin activates Toll-like receptor 4. *J Biol Chem* 2001;276:10229–33.

63 Nam J-M, Onodera Y, Bissell MJ, *et al*. Breast cancer cells in three-dimensional culture display an enhanced radioresponse after coordinate targeting of integrin alpha5beta1 and fibronectin. *Cancer Res* 2010;70:5238–48.

64 Liu W-T, Jing Y-Y, Yu G-F, *et al*. Toll like receptor 4 facilitates invasion and migration as a cancer stem cell marker in hepatocellular carcinoma. *Cancer Lett* 2015;358:136–43.

65 Fu X, Rivera A, Tao L, *et al*. Genetically modified T cells targeting neovasculature efficiently destroy tumor blood vessels, shrink established solid tumors and increase nanoparticle delivery. *Int J Cancer* 2013;133:2483–92.

66 Byrd TT, Fousek K, Pignata A, *et al*. TEM8/ANTXR1-Specific CAR T cells as a targeted therapy for triple-negative breast cancer. *Cancer Res* 2018;78:489–500.

67 Petrovic K, Robinson J, Whitworth K, *et al*. TEM8/ANTXR1-specific CAR T cells mediate toxicity in vivo. *PLoS One* 2019;14:e0224015.

68 Zhuang X, Maione F, Robinson J, *et al*. Car T cells targeting tumor endothelial marker CLEC14A inhibit tumor growth. *JCI Insight* 2020;5:e138808.

69 Chinnasamy D, Yu Z, Theoret MR, *et al*. Gene therapy using genetically modified lymphocytes targeting VEGFR-2 inhibits the growth of vascularized syngenic tumors in mice. *J Clin Invest* 2010;120:3953–68.

70 Rose DM, Grabovsky V, Alon R, *et al*. The affinity of integrin alpha(4)beta(1) governs lymphocyte migration. *J Immunol* 2001;167:2824–30.

71 Wagner J, Wickman E, Shaw TI, *et al*. Antitumor effects of CAR T cells redirected to the EDB splice variant of fibronectin. *Cancer Immunol Res* 2021;9:279–90.

72 Xie YJ, Dougan M, Jailkhani N, *et al*. Nanobody-Based CAR T cells that target the tumor microenvironment inhibit the growth of solid tumors in immunocompetent mice. *Proc Natl Acad Sci U S A* 2019;116:7624–31.